Cell

The multi-stage plasticity in the aggression circuit underlying the winner effect

Graphical abstract

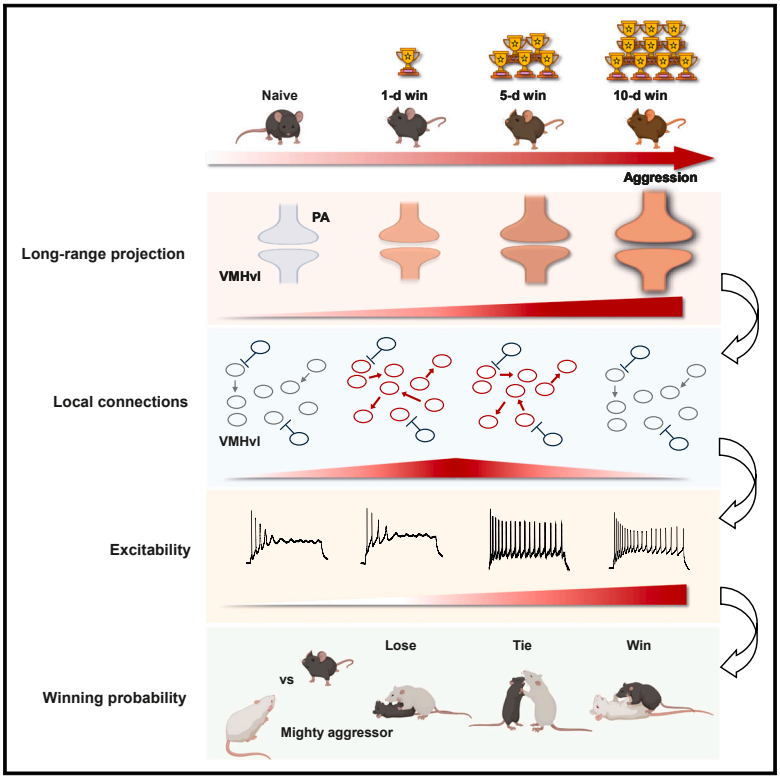

Highlights

- Over repeated winning, male mice show increased and generalized aggression
- The multi-phase plasticity of VMHvl cells supports the winner effect
- These plasticity events are causally linked
- Artificial triggering of the plasticity cascade in VMHvl cells enhances aggression

Authors

Rongzhen Yan, Dongyu Wei, Avni Varshneya, ..., Hector J. Asencio III, Aishwarya Gollamudi, Dayu Lin

Correspondence

rongzhen.yan@nyulangone.org (R.Y.), dayu.lin@nyulangone.org (D.L.)

In brief

Repeated winning increases the readiness to attack and the probability of winning, known as the winner effect. Yan et al. found that the winner effect is supported by the triple-phase plasticity of VMHvl cells, which are causally linked and triggered by the coactivation of VMHvl and PA cells during winning.

Yan et al., 2024, Cell *187*, 6785–6803
November 27, 2024
https://doi.org/10.1016/j.cell.2024.09.030

CellPress

Cell

CellPress

Article

The multi-stage plasticity in the aggression circuit underlying the winner effect

Rongzhen Yan,[1,4,*] Dongyu Wei,[1,4] Avni Varshneya,[1] Lynn Shan,[1] Bing Dai,[1] Hector J. Asencio III,[1] Aishwarya Gollamudi,[1] and Dayu Lin[1,2,3,5,*]

[1]Neuroscience Institute, New York University Langone Medical Center, New York, NY 10016, USA
[2]Department of Psychiatry, New York University Langone Medical Center, New York, NY 10016, USA
[3]Department of Neuroscience and Physiology, New York University Langone Medical Center, New York, NY 10016, USA
[4]These authors contributed equally
[5]Lead contact
*Correspondence: rongzhen.yan@nyulangone.org (R.Y.), dayu.lin@nyulangone.org (D.L.)
https://doi.org/10.1016/j.cell.2024.09.030

SUMMARY

Winning increases the readiness to attack and the probability of winning, a widespread phenomenon known as the "winner effect." Here, we reveal a transition from target-specific to generalized aggression enhancement over 10 days of winning in male mice. This behavioral change is supported by three causally linked plasticity events in the ventrolateral part of the ventromedial hypothalamus (VMHvl), a critical node for aggression. Over 10 days of winning, VMHvl cells experience monotonic potentiation of long-range excitatory inputs, transient local connectivity strengthening, and a delayed excitability increase. Optogenetically coactivating the posterior amygdala (PA) terminals and VMHvl cells potentiates the PA-VMHvl pathway and triggers the same cascade of plasticity events observed during repeated winning. Optogenetically blocking PA-VMHvl synaptic potentiation eliminates all winning-induced plasticity. These results reveal the complex Hebbian synaptic and excitability plasticity in the aggression circuit during winning, ultimately leading to increased "aggressiveness" in repeated winners.

INTRODUCTION

Aggression is an innate social behavior essential for reproduction success. The neural circuit underlying aggression is considered genetically and developmentally hardwired.[1,2] However, the readiness to express aggression varies widely among individuals in the same species, even those with identical genetic backgrounds (e.g., inbred mice). The individual difference in aggression arises partly from prior experiences, particularly winning and losing previous encounters.[3] Numerous studies have shown that winning experience heightens aggression and increases winning probability, known as the winner effect.[3]

In the last decade, the neural plasticity induced by winning and losing started to be revealed. Repeated winning in a tube test in mice enhanced the synaptic transmission from the medial thalamus to the medial prefrontal cortex, and suppressing this pathway blocked the winner effect in a tube test.[4,5] The synaptic connection from the medial thalamus to the medial prefrontal cortex was weakened in socially defeated animals.[6] In zebrafish, synaptic transmission in the lateral dorsal habenula decreased after defeat, and silencing this area eliminated the winner effect.[7]

Recent studies further revealed synaptic plasticity in subcortical regions after winning. The ventrolateral part of the ventromedial hypothalamus (VMHvl) is central for driving aggression.[8–11] Transient potentiation of glutamatergic inputs from the medial amygdala to the VMHvl is found important for the aggression escalation within 1 h after briefly interacting with a male conspecific.[12] Stagkourakis et al. found that the glutamatergic projection to the VMHvl from the posterior amygdala (PA), a region also important for aggression,[13,14] underwent synaptic potentiation after 5 days of winning.[15]

The studies above focused on the neural changes after one or a few victories. However, behavior studies revealed differential behavioral changes after short- (~3 days) vs. long-term winning (≥10 days). While both short- and long-term winning enhances aggression, long-term winners display aggressive behaviors even toward heavier and stronger males or sometimes females[16–18] and are insensitive to submissive signals from opponents.[19] Given the target- and context-unspecific attack, the long-term winners are sometimes considered "pathological."[20] Counterintuitively, some studies reported decreased total attack time of long-term winners compared with short-term winners.[21] However, when the long-term winners (20 wins) are deprived of fighting opportunities, they show a "compensatory" increase in attack duration.[21] Given the distinct features of aggressive behaviors in short- and long-term winners, we hypothesize that the aggression circuits likely undergo different changes as the winning experience accumulates.

Our study aims to investigate changes in the aggression circuit over repeated winning. We first characterized aggressive

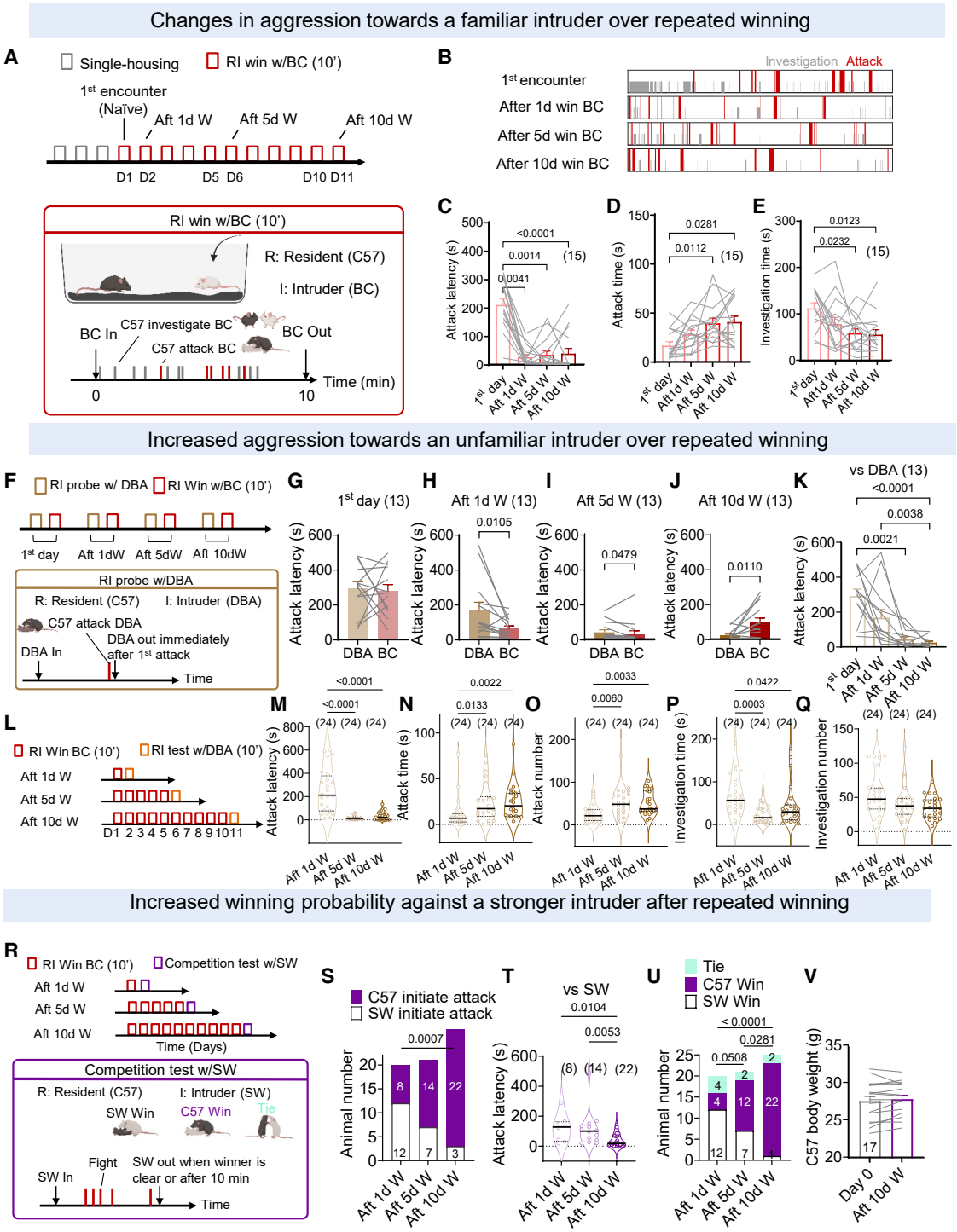

Figure 1. Changes in aggressive behaviors of male mice after repeated winning

(A) 10-day RI tests against BC male intruders. Mouse cartoons in this figure and all other figures are generated from https://www.biorender.com/.

(B) Raster plots showing attack and investigation during the RI tests.

(C–E) The latency to attack (C), attack duration (D), and social investigation duration (E) in mice with 0, 1, 5, and 10 days of winning experiences.

(F) The probe test with DBA male intruders.

(G–J) Latency to attack a familiar BC and an unfamiliar DBA intruder on the first day of RI test (G) and after a 1- (H), 5- (I), and 10-day win against BC (J).

(K) Latency to attack DBA intruders in mice with various winning experiences against BC intruders.

(L) Experimental timeline.

(legend continued on next page)

behaviors in short- and long-term winners and then investigated synaptic and cellular changes in the VMHvl over repeated winning. Our results revealed multi-phased plasticity in the VMHvl that ultimately leads to heightened aggressiveness of an animal.

RESULTS

Behavioral changes induced by repeated winning

We used repeated resident-intruder (RI) tests to provide winning experiences to the test mice. During the test, a "non-aggressive" group-housed BALB/c (BC) male mouse was introduced into the home cage of a single-housed C57BJ/6 (C57) male mouse for 10 min (Table S1). If the resident male attacked the intruder and the intruder showed flight and submissive postures, we considered the resident mouse aggressive and won. If the resident mouse investigated the intruder but did not attack during the 10-min test, we considered the resident non-aggressive and underwent "social interaction." Only animals that consistently attacked and won across days (~60% of all animals) were included in the final analysis. The 1-, 5-, and 10-day winners are animals that have experienced 1, 5, and 10 consecutive wins, respectively (not including the current RI test if relevant) (Figure 1A). Animals that showed no aggression during the 10-day RI tests constitute the social group.

The aggression increased after 1 day of winning, as indicated by the significantly shortened attack latency (Figures 1B and 1C). After 5 days of winning, the attack duration against BC reached maximum and remained similar after 10 days of winning (Figures 1C and 1D). The investigation duration decreased in 5- and 10-day winners compared with naive animals (Figure 1E).

The 1-day winning-induced aggression increase is short-lived. While the attack latency decreased the next day after 1 day of winning, it returned to the initial level if tested a week later (Figures S1A–S1E). By contrast, the aggression increase is stable in 10-day winners. After 1 week of single housing, the attack latency remained low, and the attack duration even increased, likely reflecting compensatory attack after aggression deprivation (Figures S1F–S1J).[16]

As the aggression level toward BC intruder over repeated winning could be affected by the simultaneous change in familiarity, we further probed the aggression level of naive and 1-, 5-, and 10-day winners (always win against BC) against an unfamiliar non-aggressive DBA/2NCrl (DBA) male mouse (Figures 1F–1Q; Table S1). During the probe test, the DBA intruder was removed within 5 s after the resident initiated the first attack to minimize increases in familiarity (Figure 1F). In naive mice, we found similar attack latency to BC and DBA (Figure 1G). 1-day winners (win over BC) attacked BC significantly faster than DBA, suggesting the target-specific aggression increase in this early phase of winning (Figure 1H). In 5-day winners, the latency to attack DBA and BC was similarly short (Figure 1I). Interestingly, 10-day winners attacked the unfamiliar DBA significantly faster than the familiar BC, suggesting potentially decreased aggression with increased familiarity (Figure 1J). Across the probe tests with DBA, the attack latency was significantly shorter in 5- and 10-day, but not 1-day, winners than in naive animals (Figure 1K). Additionally, we tested the behaviors of 1-, 5-, and 10-day winners (always against BC) toward unfamiliar DBA intruders in the 10-min RI tests using separate cohorts of animals so that no winner had any exposure to DBA (Figure 1L). Compared with the 1-day winners, the 5- and 10-day winners attacked the unfamiliar DBA with shorter latency and longer duration and spent less time investigating the DBA (Figures 1M–1Q). These results support a transition from target-specific to generalized aggression increase over repeated winning.

We further challenged the C57 winners with aggressive, single-housed Swiss-Webster (SW) male intruders, which are 40% heavier than the C57 and will initiate attacks even as intruders after a delay (latency to attack [mean ± STD]: 95.6 ± 33.7 s) (Table S1). We used three cohorts of C57 mice (1-, 5-, and 10-day winners against BC), and each mouse encountered the SW intruder only once (Figure 1R). As the C57 residents gained winning experience, their readiness to attack SW intruders increased (Figures 1S and 1T). 10-day winners were more likely to initiate the first attack and attack SW faster than other winner groups (Figures 1S and 1T). Importantly, 22/25 10-day winners defeated the SW, whereas only 4/20 1-day winners did so (Figure 1U). The animal's body weight did not change after the 10 days of winning, suggesting that the increased winning probability was not due to increased physical advantage (Figure 1V).

Beyond aggression, repeated winning reduced anxiety. In the novelty-suppressed feeding test, the 10-day winners ate faster and consumed more pellets than single-housed naive or social animals (Figures S2A–S2C). In a light-dark box test, the distance traveled and time spent in the light box gradually increased as the animals gained more winning experiences (Figures S2E and S2H). By contrast, mice minimally changed their performance after different days of single-housing or social interaction (Figures S2F, S2G, S2I, and S2J). The increased exploration in the light box is not due to a general increase in locomotion, as the movement velocity in home cages or a large arena did not

(M–Q) The latency to attack (M), attack duration (N), number of attacks (O), investigation duration (P), and number of investigations (Q) toward unfamiliar DBA intruders in mice with various winning experiences against BC intruders.
(R) The competition test with SW male intruders.
(S) Number of C57 and SW male mice that initiated the first attack.
(T) Latency to attack the SW in mice with various winning experiences against BC males.
(U) Number of C57 animals that win, lose, and tie with SW male intruders.
(V) Body weight of C57 male mice before and after 10 days of winning.
Numbers in parentheses or inside bars indicate the subject animal number. Circles and lines represent data of individual animals. (C, D, and K) RM Friedman test with Dunn's test. (E) RM one-way ANOVA with Tukey's test. (G and V) Paired t test. (H, I, and J) Paired Wilcoxon test. (M–Q, and T) Kruskal-Wallis test with Dunn's test. (S and U) Chi-square test. See Table S2 for detailed statistics.
In this and all other figures, black or red lines inside the violin plots mark the median; bars and error bars represent mean ± SEM; all $p \leq 0.05$ are specified; if not indicated, $p > 0.05$; all statistical tests are two-tailed.
See also Figures S1 and S2 and Table S1.

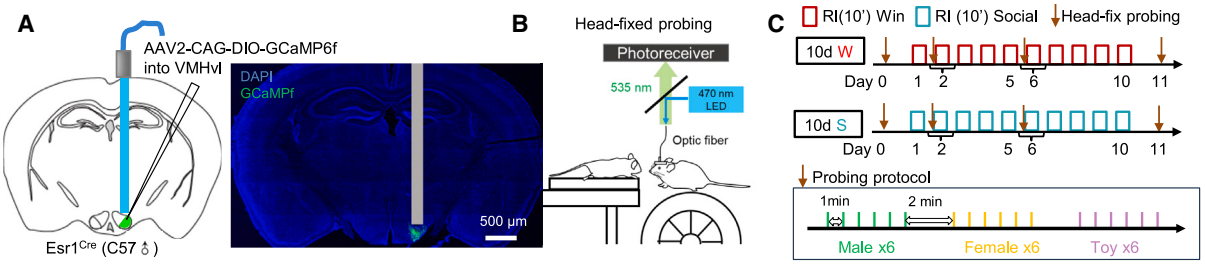

VMHvl^{Esr1} cell responses to males and females in winner group

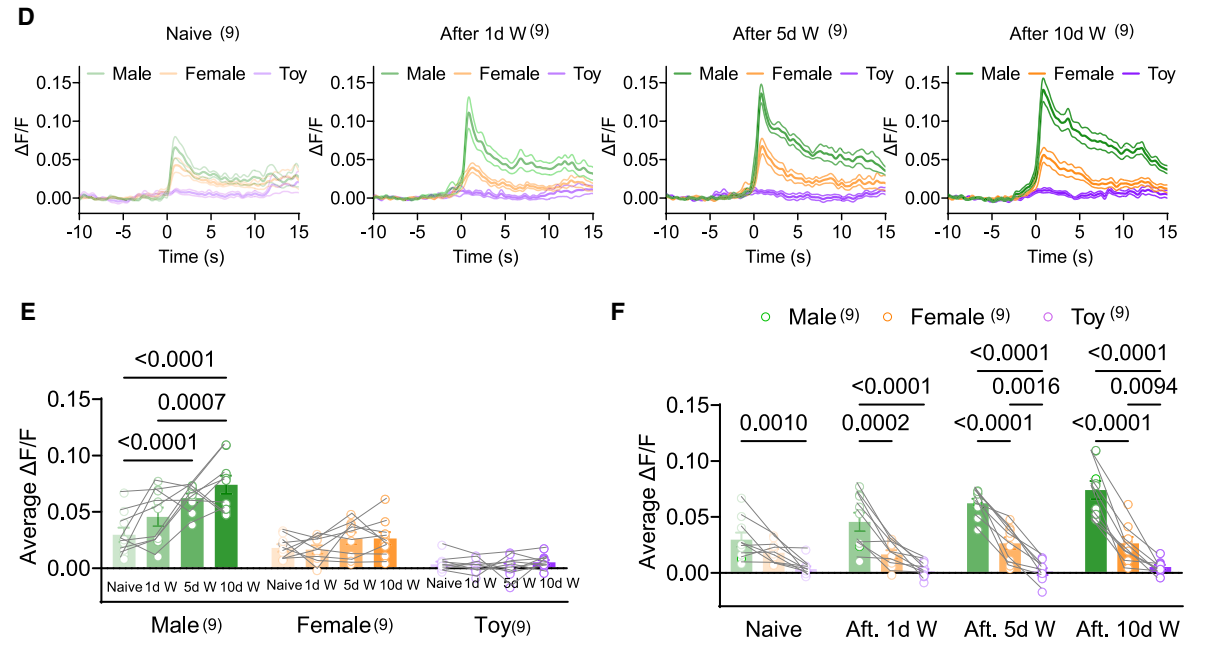

VMHvl^{Esr1} cell responses to males and females in social group

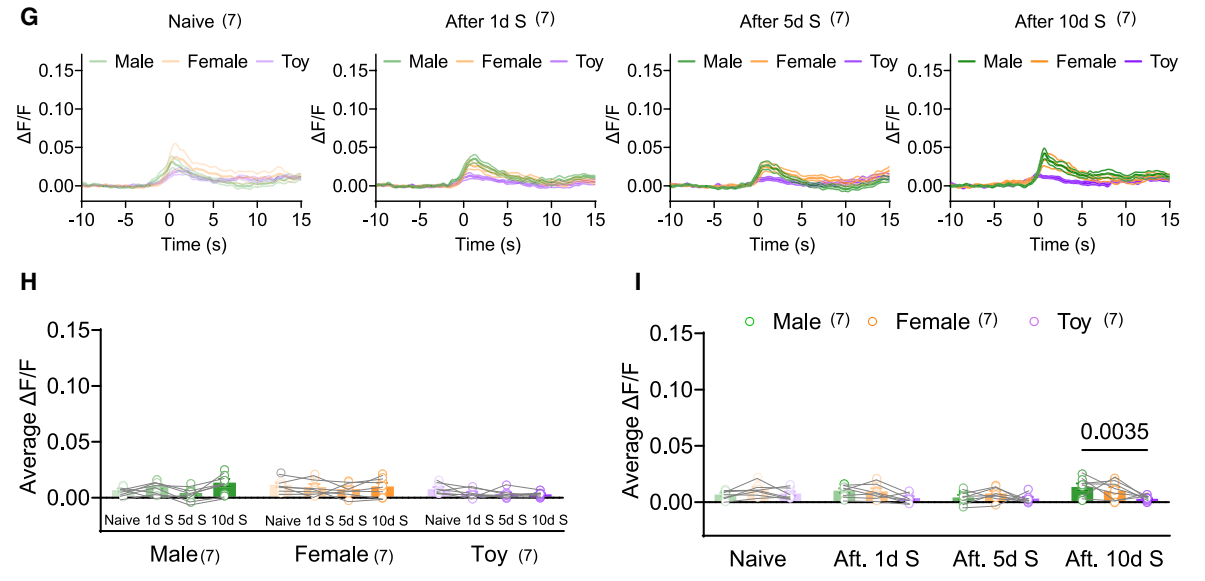

(legend on next page)

change after repeated winning (Figures S2K–S2P). Thus, repeated winning increases the animal's adventurousness.

Given the well-known role of circulating testosterone (T) in promoting male aggression[22–24] and the high levels of major urinary protein (MUP) found in dominant male mice,[25] we measured the T and MUP levels in repeated winners (Figure S2Q). Compared with naive mice, T levels increased in 5- and 10-day but not 1-day winners (Figure S2R). Similarly, MUP level showed a trend of increase in 5-day winners and rose significantly in 10-day winners (Figure S2S).

Some animals never attacked the intruder, while others became increasingly aggressive over repeated RI tests. We wondered whether any behavior or physiological parameters in naive animals could predict future aggression. Future aggressors and non-aggressors did not differ in their body weight (Figure S2T), time spent in the light box (Figure S2U), distance traveled in the light box, open field, or home cage (Figures S2V–S2X), or T level on the day before the first RI test (Figure S2Y). However, the MUP levels in the future aggressors were significantly higher than in future non-aggressors (Figure S2Z). Furthermore, the pre-attack MUP level was negatively correlated with attack latency and investigation duration (but not attack duration) on the first winning day, i.e., animals with higher MUP levels attack faster and investigate less (Figures S2AA–S2DD). Thus, MUP concentration in naive mice could indicate an animal's aggression potential while winning further increases the MUP level and causes additional neuroendocrine and behavioral changes, especially aggression.

Increase of VMHvl^{Esr1} cell responses to males over repeated winning

Changes in behaviors must be supported by changes in the underlying neural circuits. Given the critical role of estrogen receptor alpha-expressing VMHvl (VMHvl^{Esr1}) cells in generating aggression,[8–11] we examined the calcium responses of VMHvl^{Esr1} cells to aggression-provoking cues over repeated winning using fiber photometry (Figure 2A). To dissociate the behavioral and cell response changes due to winning, we presented the stimuli using a linear tracker when the recording mouse was head-fixed and awake (Figure 2B). We recorded each animal before the first RI test and after 1, 5, and 10 days of winning or social interaction (Figure 2C).

The winning experience gradually increased the VMHvl^{Esr1} cell responses to BC males (Figure 2D–2F). By contrast, VMHvl^{Esr1} cell response to females remained low (Figures 2D and 2E). Interestingly, naive animals showed no difference in VMHvl^{Esr1} cell responses to BC males vs. females, although male mice nearly exclusively attack males (Figure 2F). After winning, VMHvl^{Esr1} cells responded significantly more to males than females (Figure 2F). By contrast, the responses to both sexes remained low in non-aggressive animals after repeated social interactions (Figures 2G–2I). Regardless of the social experience, VMHvl^{Esr1} cells responded minimally to the toy mouse (Figures 2D–2I).

Changes in spontaneous synaptic transmission over repeated winning

The *in vivo* recording data supported the VMHvl as a site of change after winning. To understand whether the change occurs at the synaptic, cellular, or both levels, we performed *in vitro* patch-clamp recording of VMHvl^{Esr1} cells using brain slices obtained from single-housed naive, 1-, 5-, and 10-day winners (Figures 3A–3C). We used Esr1-zsGreen transgenic male mice to visualize Esr1-positive cells (Figure 3A).[26] The recordings were performed the day after the last RI test (Figure 3B).

Consistent with a previous report,[15] VMHvl^{Esr1} cells in 5-day winners increased spontaneous excitatory post-synaptic current (sEPSC) frequency compared with naive animals (Figures 3D and 3E). This increase also occurred in 1-day winners, suggesting its rapid onset (Figures 3D and 3E). Surprisingly, the sEPSC frequency in 10-day winners was similar to that of naive animals and significantly lower than 1- and 5-day winners (Figures 3D and 3E). In losers, we found no change in sEPSC frequency regardless of the number of losing days, while the sEPSC amplitude decreased in 10-day losers (Figures S3A–S3D). Thus, sEPSC increase in winners is not simply a consequence of fighting. To understand whether sEPSC changes are spike driven or not, we blocked action potentials using 1 μM tetrodotoxin (TTX) and examined miniature EPSC (mEPSC) and found its frequency also increased in 1- and 5-day but not 10-day winners (Figures 3G and 3H). The amplitude of sEPSC did not change in any winning groups, whereas mEPSC magnitude gradually increased and became significantly higher in 10-day winners compared with naive animals (Figures 3F and 3I). Unlike excitatory synaptic transmission, the frequency and amplitude of sIPSC and mIPSC did not differ between naive and any winning groups (Figures S3E–S3J). These results suggest dynamic and complex changes in excitatory but not inhibitory synaptic transmission over repeated winning, featuring a transient increase in mEPSC frequency and a gradual increase in mEPSC amplitude.

Spine morphology changes over repeated winning

Excitatory post-synaptic transmission occurs at dendritic spines, which are small protrusions from the dendrites.[27] The

Figure 2. VMHvl^{Esr1} cell response changes over repeated winning and social interaction

(A) Virus injection, recording site, and a histology image. Shaded rectangular marks fiber track. The brain atlases in this figure and all other figures were adapted based on a reference atlas from https://atlas.brain-map.org/.

(B) The head-fixed fiber photometry recording paradigm.

(C) Behavior and the head-fixed recording timeline.

(D and G) Average peri-stimulus time histograms (PSTHs) aligned to the onset of male, female, and toy presentation of all animals after various days of winning (D) or social interaction (G). Shades: ±SEM.

Lines represent individual animals. (E, F, H, and I) Average GCaMP responses (ΔF/F) during the male, female, and toy presentation after various days of winning (E and F) or social interaction (H and I). RM two-way ANOVA with Tukey's test.

See Table S2 for detailed statistics.

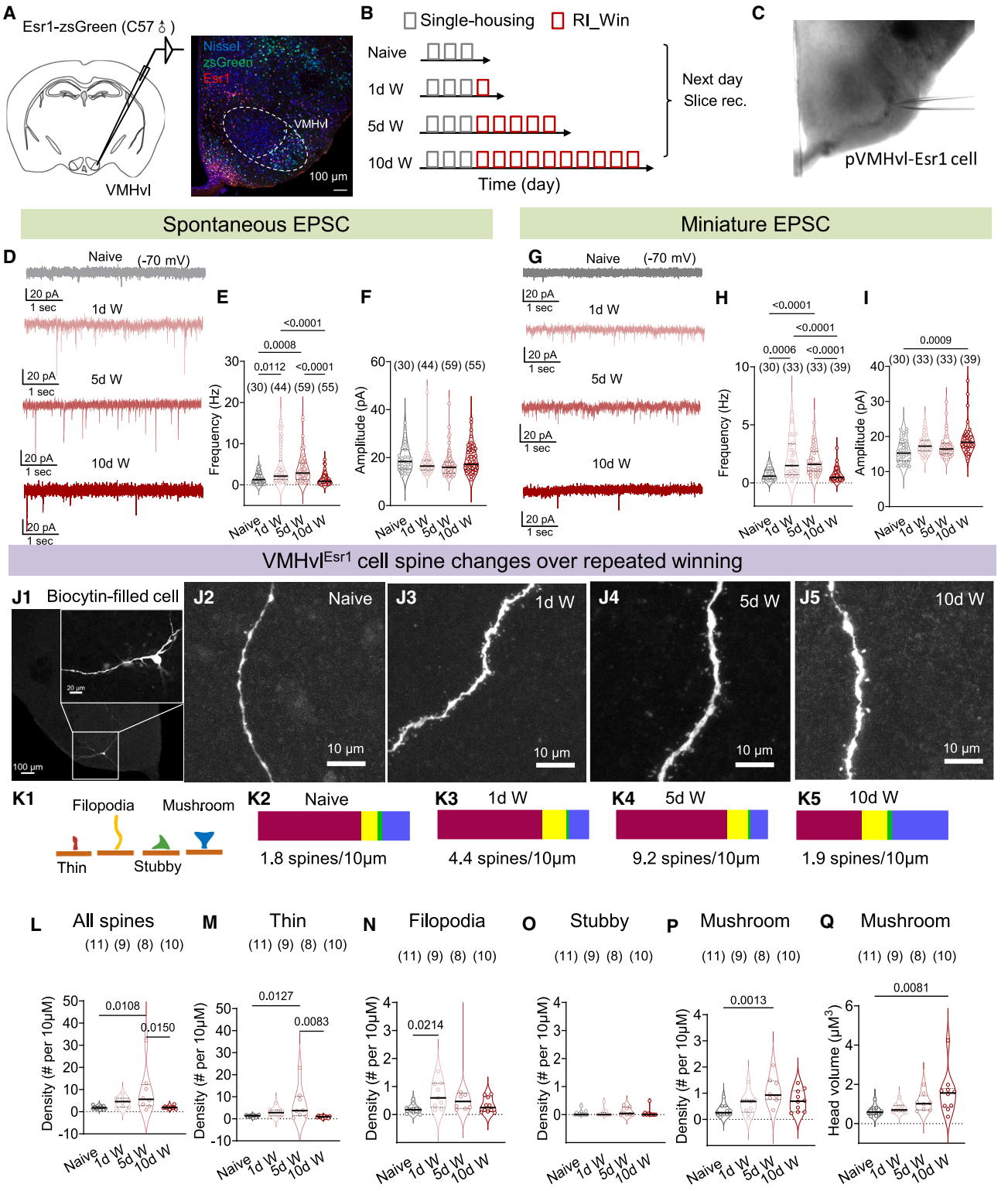

Figure 3. Synaptic transmission and spine morphology changes of VMHvl^{Esr1} cells over repeated winning

(A) Slice recording of VMHvl^{Esr1} cells and a representative histology image.

(B) Experimental timeline.

(C) A differential interference contrast (DIC) image showing a recorded VMHvl cell.

(legend continued on next page)

density of VMHvl spines is dynamically modulated.[15,28–30] Thus, we wondered whether changes in spine density can explain the up and down of m/sEPSC frequency. We filled the recorded VMHvl^{Esr1} cells with biocytin and observed a drastic increase in the spine density in 1- and 5-day but not 10-day winners (Figures 3J–3L), matching the time course of m/sEPSC frequency changes (Figures 3E and 3H).

Spines can be classified as filopodia, stubby, thin, and mushroom based on their shape and size (Figure 3K1).[31,32] Mushroom spines could be stable for months and mediate the largest synaptic current among all spines,[33] whereas other spines lasted minutes to days.[34,35] In naive animals, the overall spine density was low (1.8 spines/10 μm), and thin spines constituted 68% of all spines, followed by mushroom spines (18%), filopodia (11%), and stubby spines (3%) (Figure 3K2). In 1- and 5-day winners, the density of all types of spines increases (Figures 3L–3P). But relatively speaking, thin spines and filopodia showed larger increases than others. In 5-day winners, thin spines and filopodia increased to 87% of all spines, while the fraction of mushroom spines decreased to 12% despite its net increase in number (Figures 3K4 and 3P). In 10-day winners, all spines decreased density, but mushroom spine density decreased the least (Figures 3M–3P). Consequently, mushroom spines comprised 37% of all spines, doubling their share as in naive animals (Figures 3K2 and 3K5). Furthermore, the head volume of mushroom spines increased gradually over repeated winning and almost tripled in size in 10-day winners compared with naive animals (Figure 3Q). By contrast, 10-day social animals showed no change in spine density or morphology, suggesting the importance of winning in inducing VMHvl^{Esr1} cell plasticity (Figures S4A–S4H). These results indicate that the increased m/sEPSC frequency after short-term winning is likely due to many newly emerged spines, most unstable and disappearing in 10-day winners, causing decreased m/sEPSC frequency. However, the more stable mushroom spines survive and grow in size, likely contributing to the larger mEPSC amplitude in 10-day winners.

Increase in PA-VMHvl synaptic transmission over repeated winning

It is intriguing that some spines transiently appear while others last much longer over repeated winning. Next, we investigated the presynaptic partners of transient vs. stable spines. PA is a primary source of extra-hypothalamic excitatory input to the VMHvl, and PA-VMHvl connection was reported to strengthen after 5 days of winning.[15] Thus, we asked whether the synaptic potentiation of the PA-VMHvl pathway disappears or maintains after 10 days of winning. The former scenario will suggest PA as a source of input to the transient spines, while the latter will suggest PA partners with the longer-lasting mushroom spines.

We first examined the PA-VMHvl synaptic connection *in vitro* by expressing ChrimsonR in the PA glutamatergic cells of Esr1-zsGreen male mice and subjected the animals to single-housing alone; 1, 5, or 10 days of winning; or 10 days of social interaction (Figures 4A and 4B). We voltage-clamp recorded zsGreen-expressing VMHvl cells 4 weeks after surgery and examined the 1 ms 605 nm light-evoked EPSCs (oEPSC) (Figure 4C). The oEPSC latency was short in all groups (~3.5 ms), confirming the monosynaptic nature of the connection[13,15] (Figures 4D and 4E). However, compared with naive animals, the oEPSC amplitude showed a trend of increase in 1-day winners and became significantly higher in 5- and 10-day winners (Figure 4F). In 10-day social animals, oEPSC amplitude did not increase, suggesting the PA-VMHvl potentiation is winning-dependent (Figure 4F). In contrast to the oEPSC, light-evoked inhibitory post-synaptic current (oIPSC) amplitude did not change after winning (Figures 4G and 4I). Consistent with our previous findings,[13] the oIPSC has a long latency (~9.3 ms) and thus is likely polysynaptic (Figures 4G and 4H).

We further measured the paired-pulse ratio (PPR) and found it decreased gradually in 1-, 5-, and 10-day winners, indicating increased presynaptic release probability of PA cells over repeated winning (Figures 4J and 4K). By contrast, PPR in social animals did not differ from that in naive animals (Figures 4J and 4K). We further investigated potential changes in post-synaptic responses by measuring the relative synaptic currents mediated by α-amino-3-hydroxy-5-methylisoxazole-4-propionate (AMPA) and N-methyl-D-aspartate (NMDA) receptors. AMPA/NMDA ratio could reflect the composition of spine types as AMPA receptors are abundant in mushroom spines (up to 150/spine) but only sparsely present in thin and filopodia spines, while NMDA receptor number is similar across spines.[36] The AMPA/NMDA ratio gradually increased with repeated winning but did not change after 10 days of social interaction (Figures 4L and 4M). Thus, PA-VMHvl synaptic potentiation likely involves both pre- and post-synaptic changes.

We further monitored the strength of the PA-VMHvl pathway *in vivo* over repeated winning by expressing Chronos in PA^{Esr1} cells and implanting an optrode in the VMHvl of Esr1-2A-Cre male mice (Figures 4N and 4O).[37] 4 weeks after surgery, we probed PA to VMHvl terminal stimulation-evoked local field potential (oLFP) by delivering 5 ms, 473 nm light pulses (0.1 Hz, 120 times) to the VMHvl in naive animals. We then probed oLFPs daily for 10 consecutive days before each day's RI test (Figure 4P). oLFP amplitude increased gradually in winning mice over days but did not change in social interaction mice

(D and G) Representative voltage-clamp recording traces in ACSF (D) and 1 μM TTX (G).
(E, F, H, and I) The frequency (E and H) and amplitude (F and I) of sEPSCs (E and F) and mEPSCs (H and I) of VMHvl^{Esr1} cells in mice with various winning experiences.
(J) Representative images of a biocytin-filled VMHvl^{Esr1} cell (J1) and dendritic segments in mice with various winning experiences (J2–J5).
(K) Illustration of different spine types (K1) and the percentage of each spine type in mice with various winning experiences (K2–K5).
(L–P) Total spine density (L) and the density of thin (M), filopodia (N), stubby (O), and mushroom (P) spines of VMHvl^{Esr1} cells in mice with various winning experiences.
(Q) Head volume of mushroom spines after various winning experiences.
Circles indicate individual cells. Numbers in parentheses indicate cell numbers. (E, F, H, I, N, and O) Kruskal-Wallis test with Dunn's test. (L, M, P, and Q) One-way ANOVA with Tukey's test. See Table S2 for detailed statistics.
See also Figures S3 and S4.

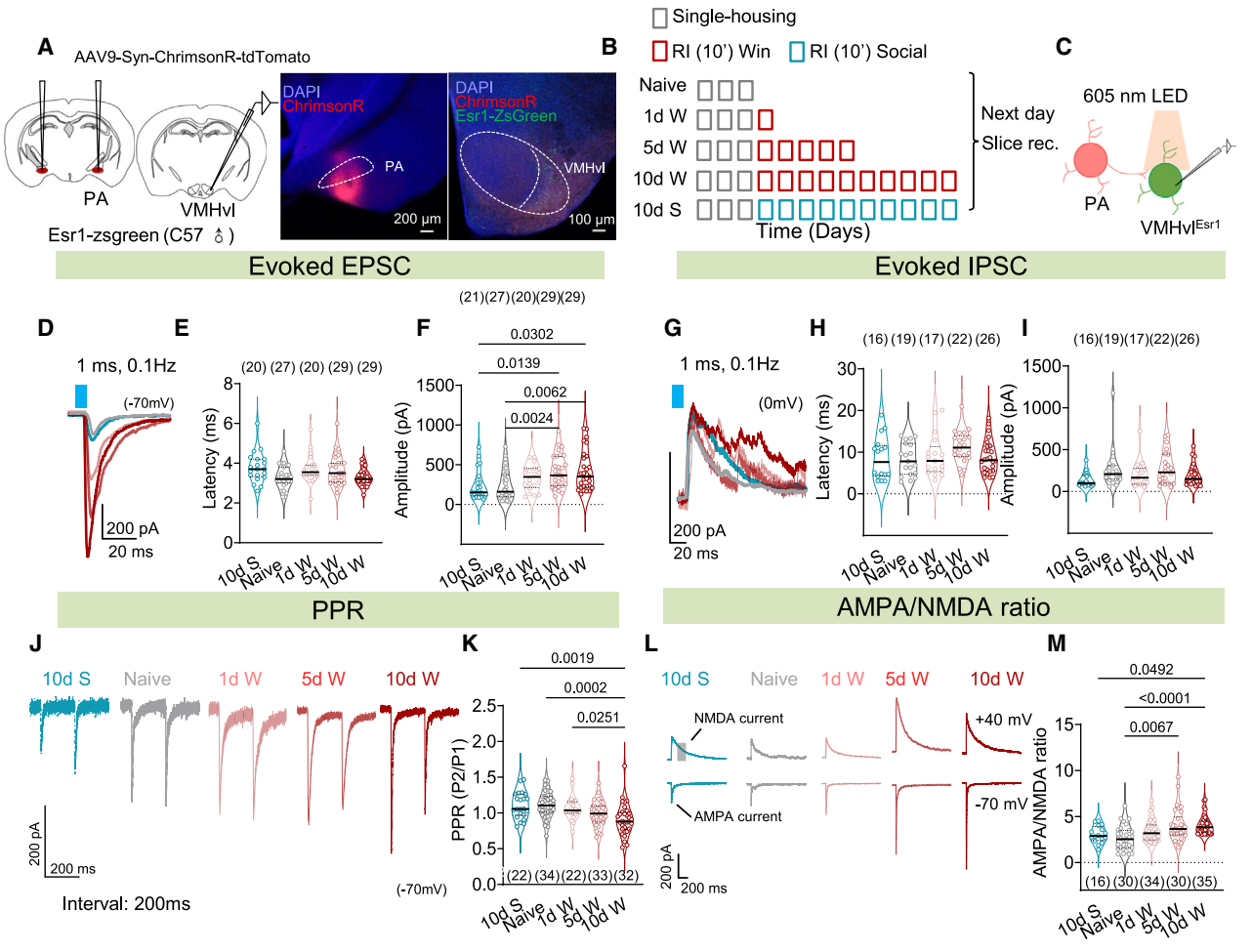

(legend on next page)

(Figures 4Q–4T). The monotonic increase in synaptic transmission from PA to VMHvl cells over 10 days of winning suggests that PA inputs likely partner with the long-lasting mushroom spines.

Transiently appeared intra-VMHvl synapses

Given that PA to VMHvl connection strengthens continuously over 10 winning days, we wonder whether the transiently appeared spines represent a qualitatively different type of connection, e.g., local connections. VMHvl^{Esr1} cells are overwhelmingly glutamatergic[9] and have been suggested to form extensive intra-VMHvl connections.[38] However, recent pair recordings revealed surprisingly sparse connections between VMHvl cells in naive animals.[39]

To test this hypothesis, we expressed Cre-dependent hM4Di-mCherry in the VMHvl^{Esr1} cells, subjected the animals to 0, 1, 5, or 10 days of winning, and performed patch-clamp recording of hM4Di-mCherry expressing VMHvl^{Esr1} cells on the day after the last win, which was timed to be approximately 3 weeks after virus injection (Figures 5A and 5B). During the recording, we bath applied clozapine-N-oxide (CNO) to block the synaptic release of hM4Di-expressing cells[40] (Figure 5C). Before CNO, as expected, sEPSC frequency in 1- and 5-day winners was higher than in naive and 10-day winners (Figure 5D–5I). After CNO, sEPSC frequency of 1- and 5-day winners, but not naive and 10-day winners, significantly decreased (Figures 5D–5H). After CNO-mediated suppression, we found no difference in sEPSC frequency across groups (Figure 5K). The sEPSC amplitude did not differ among groups regardless of CNO treatment (Figures 5J and 5L). These results suggest that first, the intra-VMHvl cell connection is likely minimal in naive animals and 10-day winners as blocking synaptic inputs from neighboring VMHvl cells has no effect on sEPSC frequency, and second, the increased sEPSC frequency in 1- and 5-day winners can be mainly accounted by the enhanced intra-VMHvl connection as blocking VMHvl inputs eliminates the increase.

Additionally, we optogenetically probed the intra-VMHvl connection *in vitro* in naive male mice, 1-, 5-, and 10-day winners using Sr^{2+} containing solution, which is less effective than Ca^{2+} and causes asynchronous and prolonged vesicle release[41] (Figures 5M–5O). Specifically, we expressed Chronos in VMHvl^{Esr1} cells and recorded quantal EPSC (qEPSC) of VMHvl^{Esr1} cells 0.5–1.5 s after optogenetic activation of neighboring presynaptic VMHvl^{Esr1} cells (Figures 5P and 5Q).[42–44] TTX (1 μM) and 4-aminopyridine (100 μM, 4AP) were added to the extracellular solutions to prevent polysynaptic EPSCs.[45] In naive animals, we found the rate of light-evoked qEPSC was low (1.02 ± 0.11 event/light pulse), supporting sparse connection among VMHvl cells (Figures 5Q and 5R). In 1- and 5-day but not 10-day winners, qEPSC frequency significantly increased, suggesting transient increases in local VMHvl connection after short-term winning (Figures 5Q and 5R). The amplitude of qEPSC in winner groups tended to be lower than in naive animals, possibly suggesting a lower glutamate load in the presynaptic ventricles of these newly formed intra-VMHvl synapses (Figure 5S).

We also expressed ChrimsonR in PA^{Esr1} cells in the same animals to record the VMHvl synaptic responses to quantal PA inputs (Figure 5T). The qEPSC frequency evoked by PA input gradually increased with repeated winning while the qEPSC amplitude stayed similar, further supporting a monotonic increase in PA-VMHvl connection strength (Figures 5U–5W). These results collectively suggest that the transient increases in mEPSC and spine density in 1- and 5-day winners likely reflect increased intra-VMHvl connection.

Changes in intrinsic properties of VMHvl^{Esr1} cells after repeated winning

The intrinsic biophysical properties of VMHvl^{Esr1} cells also changed, but only after repeated winning. We constructed frequency-current (F-I) curves of VMHvl^{Esr1} cells in mice with various winning experiences and found VMHvl^{Esr1} cells have higher firing rates in 5- and 10-day winners than naive, 1 day of winning, and 10-day social mice at nearly all current steps (Figures 6A and 6B). Between 5- and 10-day winners, the F-I curve was steeper in 10-day winners at low current steps

Figure 4. Monotonic potentiation of PA-VMHvl pathway over repeated winning

(A) Schematics of virus injection, recording site, and representative histology images.
(B) Experimental timeline.
(C) Recording schematics.
(D and G) Representative traces of oEPSC (D) and oIPSC (G) of VMHvl^{Esr1} cells from male mice with various winning experiences or 10 days of social interaction.
(E, F, H, and I) Latency (E and H) and amplitude (F and I) of oEPSC (E and F) and oIPSC (H and I) of VMHvl^{Esr1} cells from male mice with various winning experiences or 10 days of social interaction.
(J) Representative oEPSCs after two light pulses spaced by 200 ms.
(K) PPR of VMHvl^{Esr1} cells from male mice with various winning experiences or 10 days of social interaction.
(L) Representative light-evoked AMPA and NMDA currents.
(M) AMPA/NMDA ratio of VMHvl^{Esr1} cells from male mice with various winning experiences or 10 days of social interaction.
(N) The *in vivo* PA-VMHvl oLFP probing strategy.
(O) Histological image showing Chronos expression in PA and VMHvl.
(P) Timeline of behavior training and oLFP probing.
(Q) Representative oLFP traces in animals underwent repeated winning or social interaction.
(R) oLFP amplitude across days, normalized by the Bef amplitude.
(S and T) Normalized oLFP amplitude over repeated winning (S) and social interaction (T).
Circles in (E), (F), (H), (I), (K), and (M) represent individual cells. Lines in (S) and (T) represent individual animals. Numbers in parentheses represent recorded cell numbers in (E), (F), (H), (I), (K), and (M) and animal numbers in (S) and (T). (E and K) One-way ANOVA with Tukey's test. (F, H, I, and M) Kruskal-Wallis test with Dunn's test. (R) RM two-way ANOVA with Sidak's test. (S) One sample Wilcoxon test with Holm-Sidak correction and RM Friedman test with Dunn's test. (T) One sample t test with Holm-Sidak correction and RM one-way ANOVA with Tukey's test. See Table S2 for detailed statistics.

In vitro chemogenetic inhibition of intra-VMHvl connection

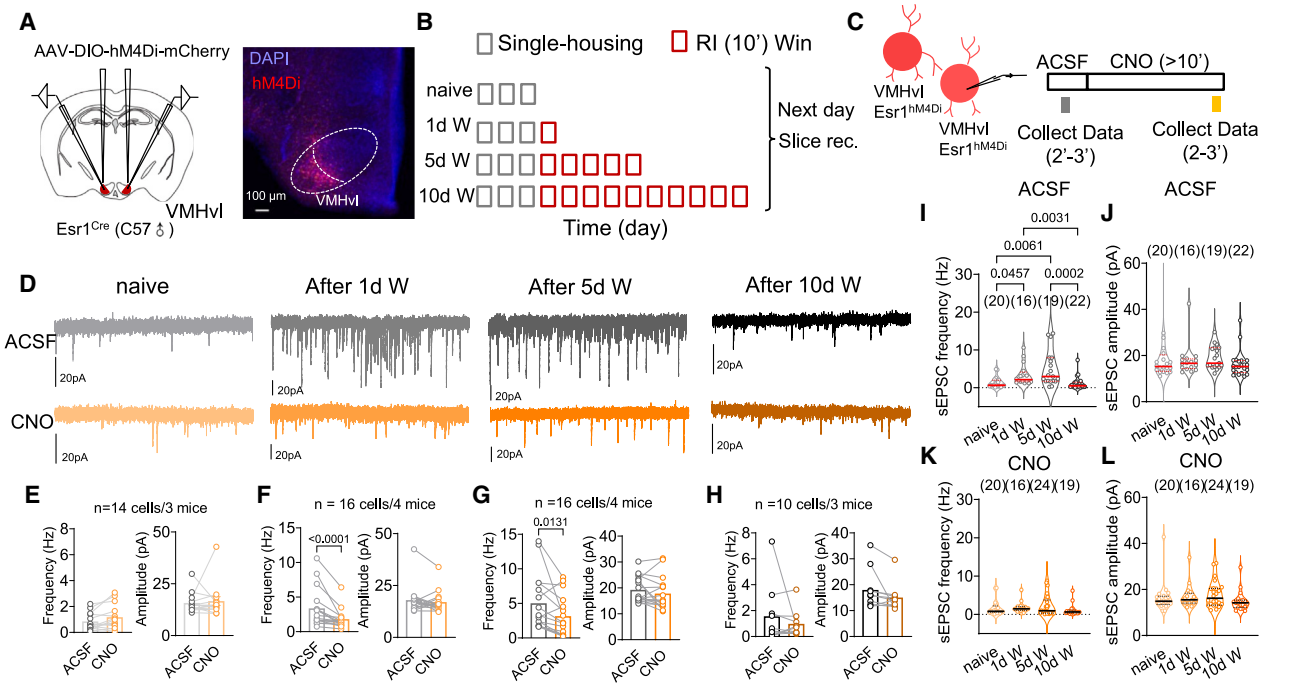

In vitro optogenetic activation of intra-VMHvl connection

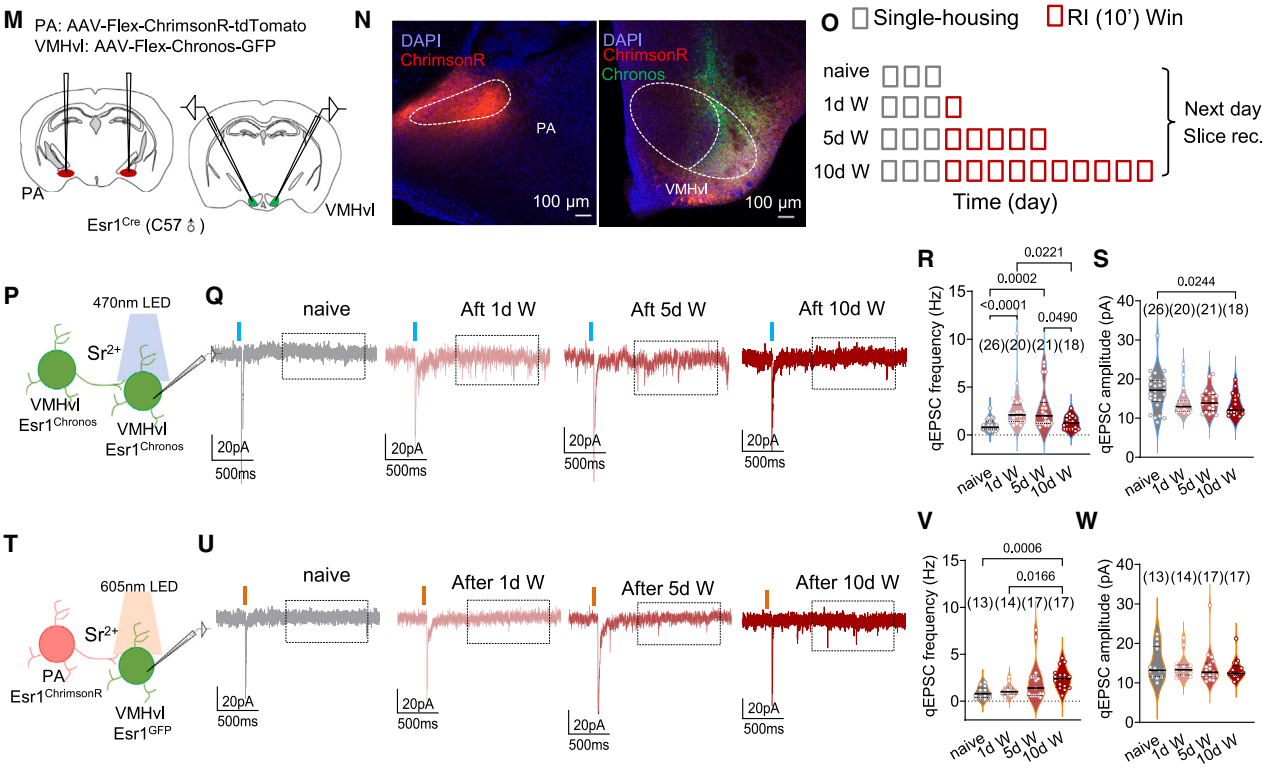

(legend on next page)

(10–30 pA), indicating increased sensitivity to small excitatory inputs (Figure 6B). In 5- and 10-day winners, the maximum firing rates and the resting membrane potential (RMP) are significantly higher than in naive animals (Figures 6A–6C and 6E). Additionally, VMHvl^{Esr1} cells in 10-day winners showed significantly decreased rheobase and increased input resistance (Figures 6D and 6F). The spiking threshold did not differ across groups (Figure 6G). None of the measured parameters in 10-day social or defeated animals differed from naive animals (Figures 6A–6G and S3K–S3Q). Thus, the VMHvl cells show increased excitability, specifically after long-term winning.

The VMHvl synaptic and intrinsic plasticity are causally linked

VMHvl cells showed three types of plasticity over 10 days of winning: continued potentiation of glutamatergic long-range inputs, transient increase of local connections, and delayed increase of cell excitability. We wondered whether these events are linked and what might be their trigger. Among the three types of plasticity, the PA-VMHvl potentiation occurs most rapidly. Immediately after the 10-min RI tests, we can detect increased PA terminal activation-evoked LFP at the VMHvl (Figures S5A–S5E). This increase is likely due to Hebbian plasticity, as PA and VMHvl cells show simultaneous activation during inter-male aggression.[13,46] Thus, we decided to test whether the PA-VMHvl potentiation alone can trigger the three plasticity events over repeated winning.

We expressed Chronos in PA^{Esr1} cells and ChrimsonR in VMHvl^{Esr1} cells and implanted an optrode in the VMHvl (Figure S5F). We then delivered 530 nm light (25 s on, 5 s off, 20 Hz, 3 times) to coactivate PA-VMHvl terminals and VMHvl cells and confirmed that this activation regime (referred to as the long-term potentiation [LTP] protocol) can rapidly increase the oLFP at the VMHvl, as described previously[15] (Figures S5G–S5J). Furthermore, repeated PA to VMHvl LTP induction once a day for 10 days caused an accumulated increase of oLFP, similar to PA-VMHvl connection change over 10 days of winning (Figures 4Q–4S and S5O–S5Q). The pre- and post-coactivation-induced acute synaptic potentiation was also observed *in vitro* at the single-cell level using patch-clamp recording (Figures S5R–S5V).

We then bilaterally expressed Chronos in PA^{Esr1} cells and ChrimsonR in VMHvl^{Esr1} cells and coactivated PA-VMHvl terminal and VMHvl cells on one side of the brain daily using the LTP protocol for 1, 5, and 10 days. The other hemisphere was unstimulated to be an internal control (Figure 7A). After 1 day of co-stimulation, the sEPSC frequency of the VMHvl^{Esr1} cells was significantly higher on the stimulated side than the control side (Figures 7D1–7E1), while the cell excitability of the two sides was similar (Figures 7G1–7H1). After 5 days of co-stimulation, both sEPSC frequency and cell excitability became significantly higher on the stimulated side than on the control side (Figures 7D2–7E2 and 7G2–7H2). Remarkably, after 10 days of co-simulation, the sEPSC frequency of the stimulated side became similarly low as the control side, while the cell excitability was significantly higher on the stimulated side (Figures 7D3–7E3 and 7G3–7H3). No difference in sEPSC amplitude was observed between the stimulation and control sides regardless of the days of stimulation, consistent with a lack of sEPSC amplitude change after winning (Figure 7F). Similar to the intrinsic property changes after a long, but not short, period of winning, we observed lower rheobase and elevated RMP of VMHvl^{Esr1} cells on the stimulated side compared with the control side after 5 and 10 days, not 1 day of co-stimulation (Figures S6A–S6C, S6E, S6F, S6H, and S6I). Furthermore, input resistance only increased after 10 days of co-stimulation, matching the time course of input resistance change over repeated winning precisely (Figures S6D, S6G, and S6J). In mice injected with the GFP or mCherry viruses into the PA and VMHvl, the cell excitability in the stimulated and control sides is similar after 10-day light delivery, suggesting that the light alone does not cause the plasticity (Figures S6K–S6O).

The morphological change after 10 days of VMHvl and PA-VMHvl coactivation also resembles that after 10 days of winning. While the total spine density of VMHvl^{Esr1} cells on the stimulated side did not differ significantly from the control side, the spine composition differed drastically (Figures S4I–S4K). The proportion of mushroom spines was 40% on the stimulated side, much higher than the 11% on the control side, due to increased mushroom spine density on the stimulated side (Figures S4J and S4O). Additionally, the mushroom spine head size was

Figure 5. Transient strengthening of intra-VMHvl connectivity over repeated winning

(A) Virus injection, recording location, and a representative histology image.
(B) Experimental timeline.
(C) Slice recording strategy to inhibit and probe intra-VMHvl connection.
(D) Representative voltage-clamp recording traces before and after 10 μM CNO perfusion.
(E–H) The frequency and amplitude of sEPSCs before and after CNO in naive mice (E) and 1- (F), 5- (G), and 10-day (H) winners.
(I–L) The frequency (I and K) and amplitude (J and L) of sEPSCs before (I and J) and after (K and L) CNO perfusion.
(M) Virus injection and recording location.
(N) Histological images showing virus expression in PA and VMHvl.
(O) Experimental timeline.
(P and T) Slice recording strategies to optogenetically probe intra-VMHvl (P) and PA-VMHvl (T) connections.
(Q and U) Representative voltage-clamp recording traces after 1 ms 470 nm light activation of VMHvl^{Esr1} cells (Q) or after 1 ms 605 nm light activation of PA terminals (U).
(R, S, V, and W) The frequency (R and V) and amplitude (S and W) of qEPSCs in response to VMHvl^{Esr1} activation (R and S) or PA terminal activation (V and W) in mice with various winning experiences.
Circles and lines represent individual recorded cells. Numbers in parentheses indicate the cell number. (E–H) Paired Wilcoxon test. (I–L, R, S, V, and W) Kruskal-Wallis test with Dunn's test. See Table S2 for detailed statistics.

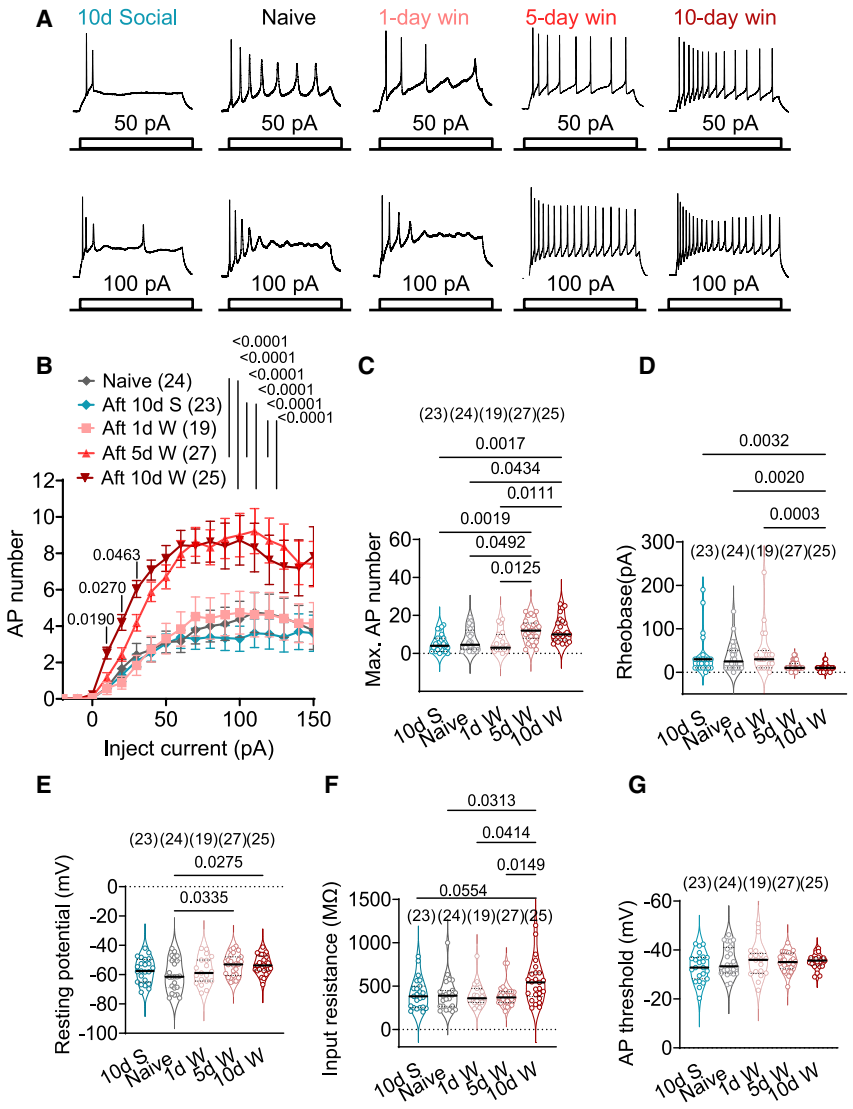

Figure 6. Increase of VMHvl^{Esr1} cell excitability after repeated winning

(A) Representative current-clamp recording traces of VMHvl^{Esr1} cells with 50 and 100 pA current injections.

(B) F-I curve of VMHvl^{Esr1} cells in mice with various winning experiences.

(C–G) Maximum action potential number across current steps (C), rheobase (D), resting membrane potential (E), input resistance (F), and action potential (AP) threshold (G) of VMHvl^{Esr1} cells in mice with various winning experiences.

Circles represent individual cells. Numbers in parentheses indicate recorded cell numbers. (B) Two-way ANOVA with Tukey's test and RM two-way ANOVA with Tukey's test. (C, D, and G) Kruskal-Wallis test with Dunn's test. (E and F) One-way ANOVA with Tukey's test. See Table S2 for detailed statistics.

See also Figure S3.

significantly larger on the stimulated side than on the control side (Figure S4P). By contrast, the density of thin spines, filopodia, and stubby spines did not differ between the two sides (Figures S4L–S4N).

To understand the necessity of PA-VMHvl potentiation in the synaptic and cellular changes induced by winning, we applied 10 min 1 Hz co-stimulation (refer as long-term depression [LTD] protocol) immediately after the RI test to block winning-induced PA-VMHvl synaptic potentiation[15] (Figures 7A and 7C). This LTD protocol effectively weakened PA-VMHvl synaptic connection *in vivo* and *in vitro* (Figures S5K–S5N and S5W–S5Z). Of note, the LTD protocol likely depresses all PA-VMHvl synapses indiscriminately.[47] Thus, it does not revert winning-induced synaptic potentiation to the naive state but is nevertheless an effective means to block PA-VMHvl potentiation. We found that sEPSC frequency was significantly higher on the control side than on the LTD side after 1-day post-winning unilateral LTD stimulation (Figures 7I–7K). The density of all spine types increased drastically on the control side, as expected from the 1-day winner, while it remained low on the LTD side (Figures S4Q–S4W). The mushroom spine head volume of the two sides was similarly low (Figure S4X).

In a separate group of mice, we performed post-winning unilateral LTD induction for 10 winning days (Figure 7C). While cells in the control side showed high excitability, as expected from 10-day winners, the LTD side showed low excitability, comparable to that of naive animals (Figures 6B, 7L, and 7M). Control animals injected with GFP and mCherry viruses showed increased cell excitability in both light-delivered and control sides (Figures S6K and S6P–S6S). Thus, PA-VMHvl synaptic potentiation is a prerequisite for the winning-induced sEPSC increase, spine growth, and excitability changes.

VMHvl synaptic plasticity is essential for aggression increase after winning

We next optogenetically applied the PA-VMHvl LTP protocol bilaterally in the naive male mice for 10 days and asked whether the induced VMHvl plasticity was sufficient to mimic the winner effect behaviorally (Figures 7O–7Q). One day before the first stimulation day, we briefly probed each animal's initial aggression level using a BC intruder. Then, after the 10-day LTP induction, we examined the behaviors toward BC, DBA, and SW intruders on separate days (Figure 7Q). The attack latency toward BC significantly decreased while the attack duration increased after 10 days of LTP induction in the opsin- but not GFP-expressing animals (Figures 7R and 7S). The BC-directed attack duration after 10-day LTP was comparable to that of 10-day winners (Figure 7S). Additionally, the 10-day LTP mice

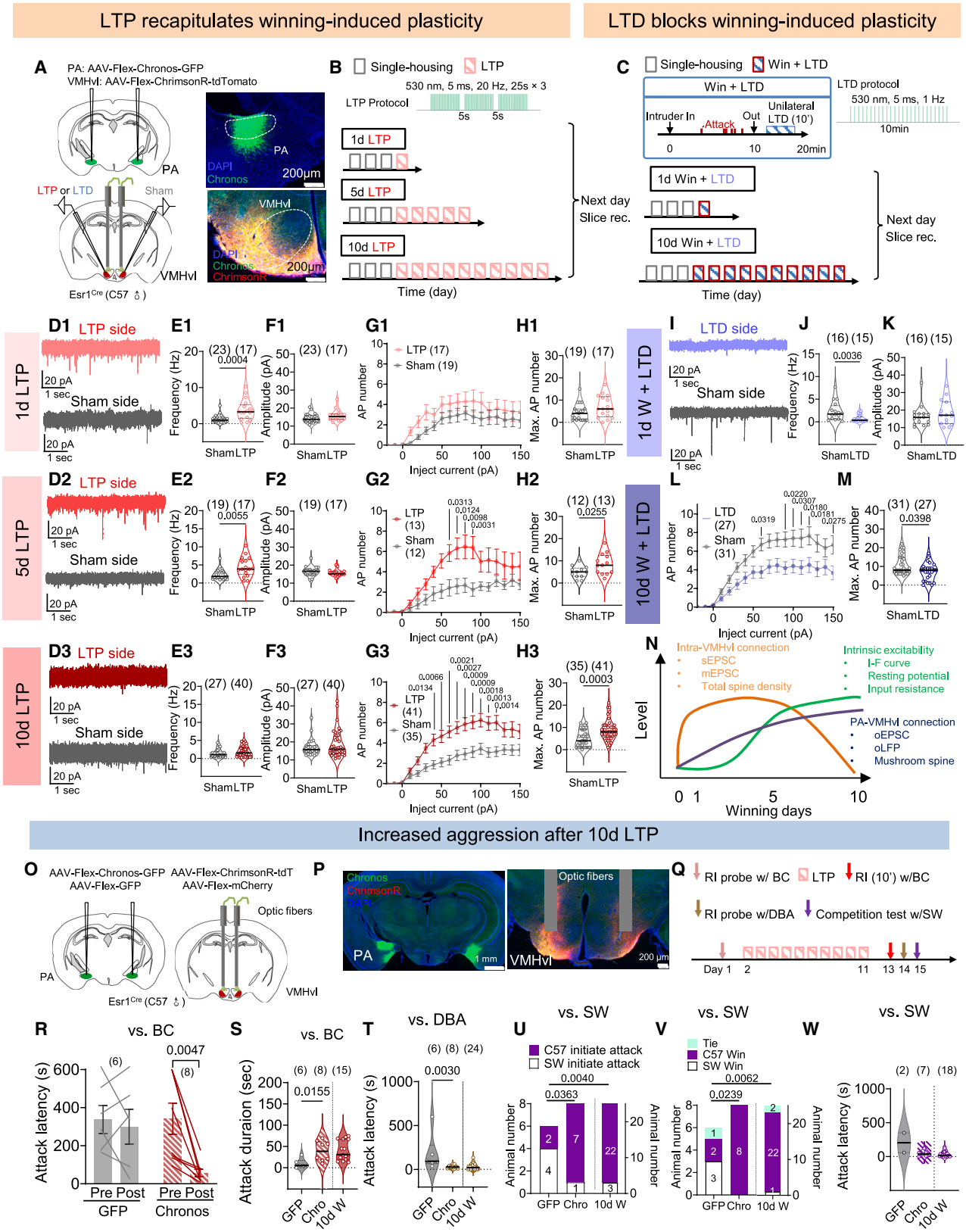

(legend on next page)

attacked an unfamiliar DBA mouse as swiftly as the 10-day winners (Figure 7T). Most strikingly, 7/8 LTP-induced mice initiated the first attack toward the SW intruders, and all 8 won the fight while only 2/6 control mice did so (Figures 7U and 7V). The SW-directed aggression in 10-day LTP mice is comparable to that of 10-day winners (Figures 7U–7W).

Given increased MUP and T levels after 10 days of winning (Figures S2R and S2S) and their suggested causal role in the winner effect,[24] we wondered whether the 10-day LTP stimulation also induces endocrine changes, which then cause the aggression increase. We collected tail blood and urine samples before and after 10 days of LTP and found no change in T and MUP levels after 10 days of LTP in both opsin and GFP groups (Figures S7A–S7C). Furthermore, the animals spent similar time and traveled approximately the same distance in the light box before and after the 10-day LTP (Figures S7A, S7D, and S7E). Thus, the cascade of plasticity at the VMHvl can support winning-induced aggression increase independent of T and MUP changes. The neural circuits beyond the VMHvl likely support changes in aggression-unrelated behaviors after repeated winning.

Lastly, to directly test the functional necessity of VMHvl synaptic plasticity in the winner effect, we injected D-APV, an NMDA receptor blocker, locally into the VMHvl after winning the RI test. In one cohort of animals, we injected D-APV to one side and vehicle to the other and performed patch-clamp recording of VMHvl cells from both sides the next day (Figure S8A). sEPSC frequency of VMHvl cells from the vehicle side was significantly higher than the D-APV side, suggesting D-APV blocked winning-induced synaptic plasticity (Figures S8B–S8D). Then, in a separate cohort of animals, we injected D-APV or vehicle bilaterally into the VMHvl after winning (Figure S8E). While the vehicle-injected animals decreased attack latency the next day, D-APV-injected animals did not (Figures S8F–S8H). Interestingly, the attack latency of D-APV animals decreased significantly on the third day after they were tested on the second day without D-APV injection (Figure S8H). Thus, NMDA receptor activation is essential for the winning-induced VMHvl cell synaptic plasticity and the winner effect.

DISCUSSION

Here, we characterized changes in aggressive behaviors over repeated winning and investigated the neuroplasticity underlying these changes. We found that as male mice gain winning experiences, they shift from low and specific aggression to high and generalized aggression, and the winning probability against a stronger opponent increase. These behavioral changes are supported by three casually linked plasticity events in the VMHvl, each with a distinct time course (Figure 7N).

The winner effect

From an ethological viewpoint, every fight allows an animal to assess its resource-holding potential (RHP) within its species.[48] Winning one fight signals the relatively high RHP of that individual within the pair. Repeated winning indicates an absolute high RHP among all individuals of the species, hence encouraging the winner to engage in future agonistic encounters more readily. Indeed, we found that after one time winning, the winning animal increases its attack specifically toward the same type of intruder that it previously defeated. As the animals win repeatedly, they show high aggression toward various intruders, even those with apparent physical superiority. In our study, however, we did not find 10-day winners attack females, which is considered pathological as it reduces reproductive success. Thus, the behaviors of the 10-day winners are likely still within the normal range of male mouse aggression.

We noticed that some animals decreased attack duration when encountering BC intruders for the 10^{th} vs. the 5^{th} time. Overall, 10-day winners attacked an unfamiliar DBA intruder faster than a familiar BC intruder. This phenomenon has been reported previously: as the animal encounters the same type of intruder repeatedly, the overt attack is replaced by other dominant behaviors, e.g., lateral threat or aggressive grooming.[16]

Figure 7. The plasticity events are causally linked and can induce the winner effect

(A) Schematic of virus injection, light delivery, and representative histology images.
(B and C) Experimental timeline of slice recordings after LTP induction (B) or post-winning LTD induction (C).
(D) Representative voltage-clamp recording traces of VMHvl^{Esr1} cells in sham and LTP sides.
(E–G) The sEPSC frequency (E), amplitude (F), and F-I curves (G) of VMHvl^{Esr1} cells in sham and LTP induction sides.
(H) The maximal action potential number across current steps of VMHvl^{Esr1} cells in sham and LTP induction sides.
(I) Representative voltage-clamp recording traces of VMHvl^{Esr1} cells in sham and LTD induction sides of a 1-day winner.
(J and K) The sEPSC frequency (J) and amplitude (K) of cells in sham and LTD sides of 1-day winners.
(L and M) F-I curve (L) and maximal action potential number (M) of VMHvl^{Esr1} cells in sham and LTD sides in 10-day winners.
(N) Temporal dynamics of three forms of VMHvl plasticity over repeated winning.
(O) *In vivo* LTP induction strategy in freely moving mice.
(P) Histology images showing virus expression and optic fiber locations.
(Q) Experimental timeline to test 10-day LTP-induced aggression change.
(R) The latency to attack BC males before and after 10-day LTP induction.
(S and T) The attack duration against BC male intruders (S) and the latency to attack DBA male intruders (T) after 10 days of LTP induction vs. 10 days of winning (against BC).
(U) The number of C57 and SW mice initiating the first attack after 10 days of LTP induction or 10 days of winning (against BC).
(V and W) The outcome of competition tests (V) and the latency to attack SW males (W) in 10-day LTP mice and 10 days of winning (against BC).
Circles in (E), (F), (H), (J), (K), and (M) represent individual cells. Circles and lines in (R)–(W) represent individual animals. Numbers inside parentheses or bars represent recorded cell numbers in (E)–(H) and (J)–(M) and subject animal numbers in (R)–(W). (E1, E2, F1, H1, H2, and S) Unpaired t test. (E3, F2, F3, H3, J, K, M, and T) Mann-Whitney test. (G1, G2, G3, L, and R) RM two-way ANOVA with Sidak's test. (U and V) Chi-square test. See Table S2 for detailed statistics.
See also Figures S4, S5, S6, S7, and S8.

Similarly, when a group of unfamiliar male mice is housed together, the fighting frequency is the highest during the first day or two and decreases once the social hierarchy is established.[49] Thus, the decreased attack toward a repeatedly encountered weaker intruder could be an adaptive behavior to reduce unnecessary fighting once the winner is clear. Importantly, the decreased attack does not indicate reduced aggressiveness. When a 10-day winner encounters an unfamiliar intruder, especially one with a higher RHP, its aggression level is clearly higher than that of 1- or 5-day winners.

The experienced winner is more likely to win against a stronger opponent, likely due to a combination of factors, such as increased attack efficiency and precision, enhanced aggressive motivation, and resilience against surrender. Our results in 10-day LTP animals suggest that aggressive motivation may dominate the winning probability in the short RI tests. Previous *in vivo* recordings reveal that VMHvl cells are activated during aggression-seeking and attack initiation but do not vary with moment-to-moment attack movements.[50,51] Thus, changes in VMHvl should mainly affect readiness to attack but not its motor performance. PA-VMHvl could also be a part of the larger circuit that modulates the resilience against surrender by determining how long the offensive attack should persist.[52]

Beyond aggression, repeated winning also enhances general adventurousness. 10-day winners are more willing to explore risky environments, e.g., the light side of a light-dark box. The VMHvl does not mediate these changes, as our 10-day LTP animals are no more adventurous than naive animals. How repeated winning affects the neural circuit beyond aggression-generation regions to change non-aggressive behaviors is an interesting topic for future studies.

The neuroplasticity in the VMHvl over repeated winning

During winning, PA and VMHvl cells are simultaneously activated, triggering a series of changes in VMHvl cells. First, within minutes of winning, the PA-VMHvl excitatory synapses are potentiated, as revealed by increased PA-VMHvl terminal stimulation-evoked LFP at the VMHvl. Similar PA-VMHvl potentiation can be induced by simply coactivating PA-VMHvl terminals and VMHvl cells for less than 2 min, suggesting the high efficiency of pre- and post-synaptic coactivation to trigger plasticity. Over 10 days of winning, the PA-VMHvl connection is continuously and monotonically strengthened, likely due to combined changes at presynaptic, e.g., increased releasing probability, and post-synaptic sites, e.g., increased AMPA receptor density. In 10-day winners, the number of mushroom spines increases significantly, some of which likely partner with PA axons as artificial PA-VMHvl pathway potentiation similarly increases the mushroom spine density, whereas PA-VMHvl depression prevents the mushroom spine increase after repeated winning.

PA represents the primary extra-hypothalamic inputs to the VMHvl. Other long-range inputs, including those from the principal nucleus bed nucleus of the stria terminalis (BNSTpr), medial amygdala, and ventral lateral septum are mainly GABAergic.[13] The other major source of glutamatergic inputs to the VMHvl arises from the ventral premammillary nucleus (PMv), situated just posterior to the VMHvl.[53,54] PMv also promotes aggression and is activated by male chemosensory cues.[54–56] Thus, the PMv to VMHvl connection may also strengthen over repeated winning.

Surprisingly, PA-VMHvl and VMHvl coactivation also trigger plasticity unrelated to the PA-VMHvl pathway. 1 day after PA-VMHvl and VMHvl coactivation, we observed a striking increase in sEPSC frequency and VMHvl cell spine density, similar to after 1 day of winning. Most of these newly formed spines are thin spines and filopodia and disappear by the 10^{th} coactivation day, as is the case after 10 days of winning. These transient spines are likely formed among VMHvl cells, as inhibiting neighboring VMHvl cell synaptic release reduces sEPSC while activating the cells has the opposite effect in 1- and 5-day winners but not naive and 10-day winners. We speculate that the increased intra-VMHvl connection may help amplify the input, synchronize the output, or maintain the spontaneous activity of VMHvl cells once triggered. The mechanisms causing the local VMHvl connection to diminish in highly experienced winners remain unclear, possibly reflecting homeostatic plasticity to prevent runaway excitation of the VMHvl once the cell excitability increases sufficiently.

Repeated winning also causes a delayed increase in VMHvl cell excitability. PA-VMHvl and VMHvl coactivation for 10 days mimics the winning-induced excitability increase while blocking the PA-VMHvl potentiation after daily winning prevents the excitability change, suggesting the causal relationship between synaptic potentiation and intrinsic excitability increase. Previous studies in the cerebellum, hippocampus, and cortex found that experience-dependent changes in cell excitability depend on NMDA receptor activation and Ca^{2+} influx.[57–60] In our study, synaptic potentiation occurs earlier than excitability increases, suggesting intrinsic property changes require a longer-lasting Ca^{2+} increase. Intriguingly, the number of NMDA receptors across spines is similar.[36] Thus, the transiently appearing local spines may be a prerequisite to increased excitability by elevating and maintaining a high intracellular Ca^{2+} level.

In contrast to popular belief[24,61](but see Demas et al.[62] for examples of T-independent aggression change), T increase appears not required to enhance aggression or induce VMHvl plasticity after winning. The 10-day LTP protocol increases VMHvl cell excitability and inter-male aggression without altering the T level. This does not mean that T plays no role in the winner effect. Instead, its role may be permissive. For example, in the absence of T, e.g., through castration, VMHvl cells may decrease excitability drastically, causing the elimination of aggression altogether. Nevertheless, our data suggest that Hebbian plasticity instead of T increase causes enhanced aggression after winning. We speculate that T increase may be important for aggression-unrelated behavioral changes after winning, given that circuits underlying these non-social behaviors should not be activated during winning, making Hebbian plasticity unlikely. Consistent with this possibility, the 10-day LTP that causes no T change also does not alter exploratory behaviors in non-social contexts.

Neuroplasticity beyond the VMHvl that supports the winner effect

One key question is whether VMHvl is a unique site of plasticity after winning or one of the many in the aggression circuit.

Recently, we simultaneously recorded 13 limbic regions in male mice and revealed synchronized activation across many sites during attack.[46] Thus, Hebbian plasticity likely occurs not only between the PA and VMHvl but also other excitatory pathways. Indeed, PA also projects densely to MeA, BNSTpr, and PMv, which are all functionally important for generating aggression. Stagkourakis et al. compared the PMv cell properties between aggressive (3-day winning) and non-aggressive male mice and found that PMv cells in aggressive mice show higher excitability and denser intra-PMv cell connectivity.[55] Future studies should address whether the VMHvl plasticity rules apply to the PMv and other aggression-related regions.

Despite being innate, the readiness to express aggression varies hugely across individuals or within the same individual over time. Our study uncovered diverse forms of plasticity in the VMHvl over the course of winning that enhance the readiness to attack collectively. As the winning experience accumulates, the form of plasticity becomes increasingly stable, making the high aggressiveness of experienced winners a stable trait independent of fighting itself. Such biophysical coding of individuality is likely a general principle beyond aggression.[63,64]

Limitations of the study

Our *in vivo* oLFP recording does not collect signals exclusively from VMHvl^{Esr1} cells. To overcome this limitation, we supplemented our *in vivo* approach with slice recordings that can specifically target VMHvl^{Esr1} cells and examine their oEPSC changes across days. However, we cannot comprehensively cover all time points from the same mice using slice recording as we can with *in vivo* recordings. Another limitation of this study is that only male mice were used due to low aggression levels and a lack of winner effect in C57 female mice. It would be valuable to develop a behavior paradigm to recapitulate the winner effect in females in the future and investigate if the same neural plasticity events occur.

RESOURCE AVAILABILITY

Lead contact

Further information and requests for resources and reagents should be directed to and will be fulfilled by the lead contact, Dayu Lin (dayu.lin@nyulangone.org).

Materials availability

This study did not generate new unique reagents.

Data and code availability

- The relevant fiber photometry, behavior annotation, and *in vivo* and *in vitro* electrophysiological recording datasets have been deposited at Zenodo (access number: 10.5281/zenodo.13732531) and are publicly available as of the date of publication.
- All MATLAB codes generated in this manuscript have been deposited at Zenodo (access number: 10.5281/zenodo.13732531) and are publicly available as of the date of publication.
- Raw behavioral videos or any additional information needed to reanalyze the data reported in this paper is available from the lead contact upon request.

ACKNOWLEDGMENTS

We thank all of the members from the Lin laboratory for the discussions, Yiwen Jiang for assistance with genotyping, Xu Yong lab for kindly sharing Esr1-zsGreen transgenic mice, and Stefanos Stagkourakis for suggestions on *in vivo* LTP and LTD protocols. We thank Long Mei for assistance with brain atlas images. This research was supported by NIH grants R01MH124927, R01MH101377, U19NS107616, and R01HD116127 (D.L.) and the Vulnerable Brain Project (D.L.).

AUTHOR CONTRIBUTIONS

D.L. conceived the project, supervised the project, designed experiments, and wrote the manuscript. R.Y. co-designed experiments, performed all *in vivo* electrophysiological recording and behavior experiments and most *in vitro* electrophysiological recordings, analyzed the data, prepared figures, and co-wrote the manuscript. D.W. performed all fiber photometry recordings and some *in vitro* electrophysiological recordings. A.V., L.S., A.G., B.D., and H.J.A. assisted with behavioral analyses. A.G. assisted with histology.

DECLARATION OF INTERESTS

The authors declare no competing interests.

STAR★METHODS

Detailed methods are provided in the online version of this paper and include the following:

- KEY RESOURCES TABLE
- EXPERIMENTAL MODEL AND STUDY PARTICIPANT DETAILS
  - Mice
  - Viruses
- METHOD DETAILS
  - Stereotaxic surgery
  - Behavior tests and analysis
  - Animal tracking and behavior analysis
  - Measure MUP and testosterone
  - Fiber photometry recording
  - oLFP recording
  - In vivo optogenetic modification of PA-VMHvl pathway
  - NMDA receptor antagonist injection
  - Patch-clamp slice electrophysiological recording
  - Dendritic spine labeling and imaging
  - Immunohistochemistry
- QUANTIFICATION AND STATISTICAL ANALYSIS

SUPPLEMENTAL INFORMATION

Supplemental information can be found online at https://doi.org/10.1016/j.cell.2024.09.030.

Received: January 4, 2024
Revised: July 17, 2024
Accepted: September 18, 2024
Published: October 14, 2024

REFERENCES

1. Tinbergen, N. (1951). The Study of Instinct (Clarendon Press).
2. Lorenz, K. (1966). On Aggression (Methuen).
3. Hsu, Y., Earley, R.L., and Wolf, L.L. (2006). Modulation of aggressive behaviour by fighting experience: mechanisms and contest outcomes. Biol. Rev. Camb. Philos. Soc. *81*, 33–74. https://doi.org/10.1017/S146479310500686X.
4. Zhou, T., Zhu, H., Fan, Z., Wang, F., Chen, Y., Liang, H., Yang, Z., Zhang, L., Lin, L., Zhan, Y., et al. (2017). History of winning remodels thalamo-PFC

circuit to reinforce social dominance. Science *357*, 162–168. https://doi.org/10.1126/science.aak9726.

5. Wang, F., Zhu, J., Zhu, H., Zhang, Q., Lin, Z., and Hu, H. (2011). Bidirectional control of social hierarchy by synaptic efficacy in medial prefrontal cortex. Science *334*, 693–697. https://doi.org/10.1126/science.1209951.
6. Franklin, T.B., Silva, B.A., Perova, Z., Marrone, L., Masferrer, M.E., Zhan, Y., Kaplan, A., Greetham, L., Verrechia, V., Halman, A., et al. (2017). Prefrontal cortical control of a brainstem social behavior circuit. Nat. Neurosci. *20*, 260–270. https://doi.org/10.1038/nn.4470.
7. Chou, M.Y., Amo, R., Kinoshita, M., Cherng, B.W., Shimazaki, H., Agetsuma, M., Shiraki, T., Aoki, T., Takahoko, M., Yamazaki, M., et al. (2016). Social conflict resolution regulated by two dorsal habenular subregions in zebrafish. Science *352*, 87–90. https://doi.org/10.1126/science.aac9508.
8. Lin, D., Boyle, M.P., Dollar, P., Lee, H., Lein, E.S., Perona, P., and Anderson, D.J. (2011). Functional identification of an aggression locus in the mouse hypothalamus. Nature *470*, 221–226.
9. Hashikawa, K., Hashikawa, Y., Tremblay, R., Zhang, J., Feng, J.E., Sabol, A., Piper, W.T., Lee, H., Rudy, B., and Lin, D. (2017). Esr1(+) cells in the ventromedial hypothalamus control female aggression. Nat. Neurosci. *20*, 1580–1590. https://doi.org/10.1038/nn.4644.
10. Lee, H., Kim, D.W., Remedios, R., Anthony, T.E., Chang, A., Madisen, L., Zeng, H., and Anderson, D.J. (2014). Scalable control of mounting and attack by Esr1+ neurons in the ventromedial hypothalamus. Nature *509*, 627–632. https://doi.org/10.1038/nature13169.
11. Yang, C.F., Chiang, M.C., Gray, D.C., Prabhakaran, M., Alvarado, M., Juntti, S.A., Unger, E.K., Wells, J.A., and Shah, N.M. (2013). Sexually dimorphic neurons in the ventromedial hypothalamus govern mating in both sexes and aggression in males. Cell *153*, 896–909. https://doi.org/10.1016/j.cell.2013.04.017.
12. Nordman, J.C., Ma, X., Gu, Q., Potegal, M., Li, H., Kravitz, A.V., and Li, Z. (2020). Potentiation of Divergent Medial Amygdala Pathways Drives Experience-Dependent Aggression Escalation. J. Neurosci. *40*, 4858–4880. https://doi.org/10.1523/JNEUROSCI.0370-20.2020.
13. Yamaguchi, T., Wei, D., Song, S.C., Lim, B., Tritsch, N.X., and Lin, D. (2020). Posterior amygdala regulates sexual and aggressive behaviors in male mice. Nat. Neurosci. *23*, 1111–1124. https://doi.org/10.1038/s41593-020-0675-x.
14. Zha, X., Wang, L., Jiao, Z.L., Yang, R.R., Xu, C., and Xu, X.H. (2020). VMHvl-Projecting Vglut1+ Neurons in the Posterior Amygdala Gate Territorial Aggression. Cell Rep. *31*, 107517. https://doi.org/10.1016/j.celrep.2020.03.081.
15. Stagkourakis, S., Spigolon, G., Liu, G., and Anderson, D.J. (2020). Experience-dependent plasticity in an innate social behavior is mediated by hypothalamic LTP. Proc. Natl. Acad. Sci. USA *117*, 25789–25799. https://doi.org/10.1073/pnas.2011782117.
16. Kudryavtseva, N.N., Smagin, D.A., Kovalenko, I.L., and Vishnivetskaya, G.B. (2014). Repeated positive fighting experience in male inbred mice. Nat. Protoc. *9*, 2705–2717. https://doi.org/10.1038/nprot.2014.156.
17. Kudryavtseva, N.N., Bondar, N.P., and Alekseyenko, O.V. (2000). Behavioral correlates of learned aggression in male mice. Aggressive Behavior *26*, 386–400. https://doi.org/10.1002/1098-2337(2000)26:5<386::AID-AB4>3.0.CO;2-#.
18. Kudryavtseva, N.N. (2012). Psychopathology of Repeated (Animal) Aggression. In Encyclopedia of the Sciences of Learning, N.M. Seel, ed. (Springer), pp. 2731–2733. https://doi.org/10.1007/978-1-4419-1428-6_708.
19. Covington, H.E., 3rd, Newman, E.L., Leonard, M.Z., and Miczek, K.A. (2019). Translational models of adaptive and excessive fighting: an emerging role for neural circuits in pathological aggression. F1000Res *8*, F1000.Faculty.Rev-963. https://doi.org/10.12688/f1000research.18883.1.
20. Kudriavtseva, N.N., Bakshtanovskaia, I.V., and Avgustinovich, D.F. (1997). The effect of the repeated experience of aggression in daily confrontations on the individual and social behavior of male mice. Zh. Vyssh. Nerv. Deiat. Im. I P Pavlova *47*, 86–97.
21. Kudryavtseva, N.N., Bondar, N.P., and Avgustinovich, D.F. (2004). Effects of repeated experience of aggression on the aggressive motivation and development of anxiety in male mice. Neurosci. Behav. Physiol. *34*, 721–730. https://doi.org/10.1023/b:neab.0000036013.11705.25.
22. Dreher, J.C., Dunne, S., Pazderska, A., Frodl, T., Nolan, J.J., and O'Doherty, J.P. (2016). Testosterone causes both prosocial and antisocial status-enhancing behaviors in human males. Proc. Natl. Acad. Sci. USA *113*, 11633–11638. https://doi.org/10.1073/pnas.1608085113.
23. Barkley, M.S., and Goldman, B.D. (1977). The effects of castration and Silastic implants of testosterone on intermale aggression in the mouse. Horm. Behav. *9*, 32–48. https://doi.org/10.1016/0018-506x(77)90048-4.
24. Oyegbile, T.O., and Marler, C.A. (2005). Winning fights elevates testosterone levels in California mice and enhances future ability to win fights. Horm. Behav. *48*, 259–267. https://doi.org/10.1016/j.yhbeh.2005.04.007.
25. Lee, W., Khan, A., and Curley, J.P. (2017). Major urinary protein levels are associated with social status and context in mouse social hierarchies. Proc. Biol. Sci. *284*, 20171570. https://doi.org/10.1098/rspb.2017.1570.
26. Saito, K., He, Y., Yan, X., Yang, Y., Wang, C., Xu, P., Hinton, A.O., Jr., Shu, G., Yu, L., Tong, Q., and Xu, Y. (2016). Visualizing estrogen receptor-α-expressing neurons using a new ERα-ZsGreen reporter mouse line. Metabolism *65*, 522–532. https://doi.org/10.1016/j.metabol.2015.12.011.
27. Yuste, R., and Bonhoeffer, T. (2004). Genesis of dendritic spines: insights from ultrastructural and imaging studies. Nat. Rev. Neurosci. *5*, 24–34. https://doi.org/10.1038/nrn1300.
28. Calizo, L.H., and Flanagan-Cato, L.M. (2000). Estrogen selectively regulates spine density within the dendritic arbor of rat ventromedial hypothalamic neurons. J. Neurosci. *20*, 1589–1596.
29. Frankfurt, M., Gould, E., Woolley, C.S., and McEwen, B.S. (1990). Gonadal steroids modify dendritic spine density in ventromedial hypothalamic neurons: a Golgi study in the adult rat. Neuroendocrinology *51*, 530–535. https://doi.org/10.1159/000125387.
30. Dias, I.C., Gutierrez-Castellanos, N., Ferreira, L., and Lima, S.Q. (2021). The Structural and Electrophysiological Properties of Progesterone Receptor-Expressing Neurons Vary along the Anterior-Posterior Axis of the Ventromedial Hypothalamus and Undergo Local Changes across the Reproductive Cycle. eNeuro *8*, ENEURO.0049-21.2021. https://doi.org/10.1523/ENEURO.0049-21.2021.
31. Pchitskaya, E., and Bezprozvanny, I. (2020). Dendritic Spines Shape Analysis-Classification or Clusterization? Perspective. Front. Synaptic Neurosci. *12*, 31. https://doi.org/10.3389/fnsyn.2020.00031.
32. Ghani, M.U., Mesadi, F., Kanık, S.D., Argunşah, A.Ö., Hobbiss, A.F., Israely, I., Ünay, D., Taşdizen, T., and Çetin, M. (2017). Dendritic spine classification using shape and appearance features based on two-photon microscopy. J. Neurosci. Methods *279*, 13–21. https://doi.org/10.1016/j.jneumeth.2016.12.006.
33. Grutzendler, J., Kasthuri, N., and Gan, W.B. (2002). Long-term dendritic spine stability in the adult cortex. Nature *420*, 812–816. https://doi.org/10.1038/nature01276.
34. Ziv, N.E., and Smith, S.J. (1996). Evidence for a role of dendritic filopodia in synaptogenesis and spine formation. Neuron *17*, 91–102. https://doi.org/10.1016/s0896-6273(00)80283-4.
35. Holtmaat, A.J.G.D., Trachtenberg, J.T., Wilbrecht, L., Shepherd, G.M., Zhang, X., Knott, G.W., and Svoboda, K. (2005). Transient and persistent dendritic spines in the neocortex in vivo. Neuron *45*, 279–291. https://doi.org/10.1016/j.neuron.2005.01.003.
36. Matsuzaki, M., Ellis-Davies, G.C., Nemoto, T., Miyashita, Y., Iino, M., and Kasai, H. (2001). Dendritic spine geometry is critical for AMPA receptor expression in hippocampal CA1 pyramidal neurons. Nat. Neurosci. *4*, 1086–1092. https://doi.org/10.1038/nn736.

37. Klapoetke, N.C., Murata, Y., Kim, S.S., Pulver, S.R., Birdsey-Benson, A., Cho, Y.K., Morimoto, T.K., Chuong, A.S., Carpenter, E.J., Tian, Z., et al. (2014). Independent optical excitation of distinct neural populations. Nat. Methods *11*, 338–346. https://doi.org/10.1038/nmeth.2836.

38. Nishizuka, M., and Pfaff, D.W. (1989). Intrinsic synapses in the ventromedial nucleus of the hypothalamus: an ultrastructural study. J. Comp. Neurol. *286*, 260–268. https://doi.org/10.1002/cne.902860210.

39. Shao, Y.Q., Fan, L., Wu, W.Y., Zhu, Y.J., and Xu, H.T. (2022). A developmental switch between electrical and neuropeptide communication in the ventromedial hypothalamus. Curr. Biol.: CB *32*, 3137–3145.e3133. https://doi.org/10.1016/j.cub.2022.05.029.

40. Stachniak, T.J., Ghosh, A., and Sternson, S.M. (2014). Chemogenetic synaptic silencing of neural circuits localizes a hypothalamus→midbrain pathway for feeding behavior. Neuron *82*, 797–808. https://doi.org/10.1016/j.neuron.2014.04.008.

41. Abdul-Ghani, M.A., Valiante, T.A., and Pennefather, P.S. (1996). Sr2+ and quantal events at excitatory synapses between mouse hippocampal neurons in culture. J. Physiol. *495*, 113–125. https://doi.org/10.1113/jphysiol.1996.sp021578.

42. Bekkers, J.M., and Clements, J.D. (1999). Quantal amplitude and quantal variance of strontium-induced asynchronous EPSCs in rat dentate granule neurons. J. Physiol. *516*, 227–248. https://doi.org/10.1111/j.1469-7793.1999.227aa.x.

43. Lee, J.-H., Kim, W.B., Park, E.H., and Cho, J.-H. (2023). Neocortical synaptic engrams for remote contextual memories. Nat. Neurosci. *26*, 259–273. https://doi.org/10.1038/s41593-022-01223-1.

44. Keppeler, D., Merino, R.M., Lopez de la Morena, D., Bali, B., Huet, A.T., Gehrt, A., Wrobel, C., Subramanian, S., Dombrowski, T., Wolf, F., et al. (2018). Ultrafast optogenetic stimulation of the auditory pathway by targeting-optimized Chronos. EMBO J. *37*, e99649. https://doi.org/10.15252/embj.201899649.

45. Petreanu, L., Mao, T., Sternson, S.M., and Svoboda, K. (2009). The subcellular organization of neocortical excitatory connections. Nature *457*, 1142–1145. https://doi.org/10.1038/nature07709.

46. Guo, Z., Yin, L., Diaz, V., Dai, B., Osakada, T., Lischinsky, J.E., Chien, J., Yamaguchi, T., Urtecho, A., Tong, X., et al. (2023). Neural dynamics in the limbic system during male social behaviors. Neuron *111*, 3288–3306.e4. https://doi.org/10.1016/j.neuron.2023.07.011.

47. Mockett, B., Coussens, C., and Abraham, W.C. (2002). NMDA receptor-mediated metaplasticity during the induction of long-term depression by low-frequency stimulation. Eur. J. Neurosci. *15*, 1819–1826. https://doi.org/10.1046/j.1460-9568.2002.02008.x.

48. Parker, G.A. (1974). Assessment strategy and the evolution of fighting behaviour. J. Theor. Biol. *47*, 223–243. https://doi.org/10.1016/0022-5193(74)90111-8.

49. Williamson, C.M., Lee, W., and Curley, J.P. (2016). Temporal dynamics of social hierarchy formation and maintenance in male mice. Anim. Behav. *115*, 259–272. https://doi.org/10.1016/j.anbehav.2016.03.004.

50. Mei, L., Osakada, T., and Lin, D. (2023). Hypothalamic control of innate social behaviors. Science *382*, 399–404. https://doi.org/10.1126/science.adh8489.

51. Falkner, A.L., Grosenick, L., Davidson, T.J., Deisseroth, K., and Lin, D. (2016). Hypothalamic control of male aggression-seeking behavior. Nat. Neurosci. *19*, 596–604. https://doi.org/10.1038/nn.4264.

52. Nakajo, H., Chou, M.Y., Kinoshita, M., Appelbaum, L., Shimazaki, H., Tsuboi, T., and Okamoto, H. (2020). Hunger Potentiates the Habenular Winner Pathway for Social Conflict by Orexin-Promoted Biased Alternative Splicing of the AMPA Receptor Gene. Cell Rep. *31*, 107790. https://doi.org/10.1016/j.celrep.2020.107790.

53. Lo, L., Yao, S., Kim, D.W., Cetin, A., Harris, J., Zeng, H., Anderson, D.J., and Weissbourd, B. (2019). Connectional architecture of a mouse hypothalamic circuit node controlling social behavior. Proc. Natl. Acad. Sci. USA *116*, 7503–7512. https://doi.org/10.1073/pnas.1817503116.

54. Soden, M.E., Miller, S.M., Burgeno, L.M., Phillips, P.E.M., Hnasko, T.S., and Zweifel, L.S. (2016). Genetic Isolation of Hypothalamic Neurons that Regulate Context-Specific Male Social Behavior. Cell Rep. *16*, 304–313. https://doi.org/10.1016/j.celrep.2016.05.067.

55. Stagkourakis, S., Spigolon, G., Williams, P., Protzmann, J., Fisone, G., and Broberger, C. (2018). A neural network for intermale aggression to establish social hierarchy. Nat. Neurosci. *21*, 834–842. https://doi.org/10.1038/s41593-018-0153-x.

56. Chen, A.X., Yan, J.J., Zhang, W., Wang, L., Yu, Z.X., Ding, X.J., Wang, D.Y., Zhang, M., Zhang, Y.L., Song, N., et al. (2020). Specific Hypothalamic Neurons Required for Sensing Conspecific Male Cues Relevant to Intermale Aggression. Neuron *108*, 763–774.e6. https://doi.org/10.1016/j.neuron.2020.08.025.

57. Armano, S., Rossi, P., Taglietti, V., and D'Angelo, E. (2000). Long-term potentiation of intrinsic excitability at the mossy fiber-granule cell synapse of rat cerebellum. J. Neurosci. *20*, 5208–5216. https://doi.org/10.1523/jneurosci.20-14-05208.2000.

58. Aizenman, C.D., and Linden, D.J. (2000). Rapid, synaptically driven increases in the intrinsic excitability of cerebellar deep nuclear neurons. Nat. Neurosci. *3*, 109–111. https://doi.org/10.1038/72049.

59. Zhang, W., and Linden, D.J. (2003). The other side of the engram: experience-driven changes in neuronal intrinsic excitability. Nat. Rev. Neurosci. *4*, 885–900. https://doi.org/10.1038/nrn1248.

60. Debanne, D., Inglebert, Y., and Russier, M. (2019). Plasticity of intrinsic neuronal excitability. Curr. Opin. Neurobiol. *54*, 73–82. https://doi.org/10.1016/j.conb.2018.09.001.

61. Batrinos, M.L. (2012). Testosterone and aggressive behavior in man. Int. J. Endocrinol. Metab. *10*, 563–568.

62. Demas, G.E., Munley, K.M., and Jasnow, A.M. (2023). A seasonal switch hypothesis for the neuroendocrine control of aggression. Trends Endocrinol. Metab. *34*, 799–812. https://doi.org/10.1016/j.tem.2023.08.015.

63. Mei, L., Yan, R., Yin, L., Sullivan, R.M., and Lin, D. (2023). Antagonistic circuits mediating infanticide and maternal care in female mice. Nature *618*, 1006–1016. https://doi.org/10.1038/s41586-023-06147-9.

64. Ammari, R., Monaca, F., Cao, M., Nassar, E., Wai, P., Del Grosso, N.A., Lee, M., Borak, N., Schneider-Luftman, D., and Kohl, J. (2023). Hormone-mediated neural remodeling orchestrates parenting onset during pregnancy. Science *382*, 76–81. https://doi.org/10.1126/science.adi0576.

65. Kraeuter, A.K., Guest, P.C., and Sarnyai, Z. (2019). The Open Field Test for Measuring Locomotor Activity and Anxiety-Like Behavior. Methods Mol. Biol. *1916*, 99–103. https://doi.org/10.1007/978-1-4939-8994-2_9.

66. Takao, K., and Miyakawa, T. (2006). Light/dark transition test for mice. J. Vis. Exp. *1*, 104.

67. Blasco-Serra, A., González-Soler, E.M., Cervera-Ferri, A., Teruel-Martí, V., and Valverde-Navarro, A.A. (2017). A standardization of the Novelty-Suppressed Feeding Test protocol in rats. Neurosci. Lett. *658*, 73–78. https://doi.org/10.1016/j.neulet.2017.08.019.

68. Ning, L., Suleiman, H.Y., and Miner, J.H. (2020). Synaptopodin Is Dispensable for Normal Podocyte Homeostasis but Is Protective in the Context of Acute Podocyte Injury. J. Am. Soc. Nephrol. *31*, 2815–2832. https://doi.org/10.1681/asn.2020050572.

69. Zhang, J., Dong, X.J., Ding, M.R., You, C.Y., Lin, X., Wang, Y., Wu, M.J.Y., Xu, G.F., and Wang, G.D. (2020). Resveratrol decreases high glucose-induced apoptosis in renal tubular cells via suppressing endoplasmic reticulum stress. Mol. Med. Rep. *22*, 4367–4375. https://doi.org/10.3892/mmr.2020.11511.

70. Yoo, S., Cha, D., Kim, S., Jiang, L., Cooke, P., Adebesin, M., Wolfe, A., Riddle, R., Aja, S., and Blackshaw, S. (2020). Tanycyte ablation in the arcuate nucleus and median eminence increases obesity susceptibility by increasing body fat content in male mice. Glia *68*, 1987–2000. https://doi.org/10.1002/glia.23817.

71. Wong, L.C., Wang, L., D'Amour, J.A., Yumita, T., Chen, G., Yamaguchi, T., Chang, B.C., Bernstein, H., You, X., Feng, J.E., et al. (2016). Effective Modulation of Male Aggression through Lateral Septum to Medial Hypothalamus Projection. Curr. Biol. *26*, 593–604. https://doi.org/10.1016/j.cub.2015.12.065.

72. Yin, L., Hashikawa, K., Hashikawa, Y., Osakada, T., Lischinsky, J.E., Diaz, V., and Lin, D. (2022). VMHvlCckar cells dynamically control female sexual behaviors over the reproductive cycle. Neuron *110*, 3000–3017.e8. https://doi.org/10.1016/j.neuron.2022.06.026.

73. Wei, D., Osakada, T., Guo, Z., Yamaguchi, T., Varshneya, A., Yan, R., Jiang, Y., and Lin, D. (2023). A hypothalamic pathway that suppresses aggression toward superior opponents. Nat. Neurosci. *26*, 774–787. https://doi.org/10.1038/s41593-023-01297-5.

STAR★METHODS

KEY RESOURCES TABLE

REAGENT or RESOURCE	SOURCE	IDENTIFIER
Antibodies		
Rabbit anti-Esr1	Millipore	Cat# 06-935; RRID: AB_310305
Cy3 donkey anti-rabbit IgG	Jackson Immuno Research	Cat# 711-165-152; RRID: AB_2307443
Bacterial and virus strains		
AAV2-EF1a-Flex-Chronos-GFP	UNC Vector Core	Cat# AV6561B
AAV2-Syn-Flex-ChrimsonR-tdTomato	UNC Vector Core	Cat# AV6555B
AAV2-CAG-Flex-GCaMP6f-WPRE-SV40	UPenn Vector Core	Cat# V7478S
AAV5-Syn-Chronos-GFP	Addgene	Cat# 59170-AAV5
AAV2-hSyn-DIO-hM4Di-mCherry	Addgene	Cat# 44362-AAV2
AAV2-hSyn-Flex-GFP	UNC Vector Core	Cat# AV4530B and AV4530C
AAV2-hSyn-DIO-mCherry	Addgene	Cat# 50459-AAV2
AAV9-Syn-ChrimsonR-tdTomato	Addgene	Cat# 59171-AAV9
Chemicals, peptides, and recombinant proteins		
D-APV	Tocris	Cat# 0106
CNO	Tocris	Cat# 6329
TTX	Tocris	Cat# 1069
4AP	Tocris	Cat# 0940
SR-95531 hydrobromide	Tocris	Cat# 1262
Biocytin	Tocris	Cat# 3349
Streptavidin, Alexa Fluor™ 647 conjugate	Thermo Fisher Scientific	Cat# S21374; RRID: AB_2336066
NeuroTrace™ 435/455 Blue Fluorescent Nissl Stain	Thermo Fisher Scientific	Cat# N21479
Critical commercial assays		
QuantiChrom Protein Creatinine Ratio Assay Kit	BioAssay Systems	Cat# DPCR-100
Mouse Testosterone ELISA Kit	Crystal Chem	Cat# 80552
Experimental models: Organisms/strains		
C57BL/6 mice	Charles River	Strain Code 027
DBA/2 mice	Charles River	Strain Code 026
BALB/c mice	Charles River	Strain Code 028
Swiss Webster mice	Taconic	N/A
Esr1-zsGreen mice	Yong Yu lab, Saito et al.[26]	N/A
Software and algorithms		
Neurolucida 360	MBF Bioscience	https://www.mbfbioscience.com/products/neurolucida-360; RRID: SCR_016788
Neurolucida Explorer	MBF Bioscience	https://www.mbfbioscience.com/products/neurolucida-explorer; RRID: SCR_017348
pClamp	Molecular Devices	https://www.moleculardevices.com/; RRID: SCR_011323
Clampfit	Molecular Devices	https://www.moleculardevices.com/; Version: v10.7 and v11.2
Prism	GraphPad Software	https://www.graphpad.com/features; RRID: SCR_005375
MATLAB	MathWorks	https://www.mathworks.com/products/matlab.html; RRID: SCR_001622

(*Continued on next page*)

Continued

REAGENT or RESOURCE	SOURCE	IDENTIFIER
Any-maze software	Stoelting	https://stoeltingco.com/Neuroscience/ANY-maze; RRID: SCR_014289
StreamPix	Norpix	https://www.norpix.com/products/streampix/streampix.php; RRID: SCR_015773
Other		
473nm laser	Shanghai Dream Lasers Technology Co., Ltd.	http://www.dreamlasers.cn/; Cat# SDL-473-100MFL
530nm laser	Changchun New Industries Optoelectronics Technology Co., Ltd.	https://www.cnioptics.com/; Cat# PSU-III-LED
Light-dark box	Stoelting	https://stoeltingco.com/Neuroscience/LightDark-Box~9857?navigate_from_document=1179&navigated_from_object=3999; Cat# 63101
Open-field box	Stoelting	https://stoeltingco.com/Neuroscience/Open-Field~9839?navigate_from_document=1182&navigated_from_object=4002; Cat# 60101
Fiber photometry system	TDT	http://www.tdt.com/; RRID: SCR_006495

EXPERIMENTAL MODEL AND STUDY PARTICIPANT DETAILS

Mice

All procedures were approved by the NYULMC Institutional Animal Care and Use Committee (IACUC) in compliance with the NIH guidelines for the care and use of laboratory animals. All mice used in this study were housed under a 12h light-dark cycle (light cycle, 10 p.m to 10 a.m.), with food and water ad libitum. Room temperature was maintained between 20-22 °C, and humidity between 30-70%, with an average of approximately 45%. $Esr1^{Cre}$ knock-in mice with C57BL/6 background were purchased from Jackson Laboratory (Stocks #017913). The Esr1-zsGreen mouse[26] was originally generated and kindly provided by Dr. Yong Xu at Baylor College of Medicine, and then it was bred in-house with C57 WT mice. Apart from the experimental animals, three strains of mice were also used as intruders in the RI tests. The group-housed BALB/c male mice (>8 weeks) were used when we aimed to provide the resident mice with winning experiences. Group-housed DBA/2 male mice (>8 weeks, Charles River) were used as unfamiliar intruders for aggression probing. Single-housed aggressive Swiss Webster male mice (>10 months, Taconic) were used as challengers to evaluate the maximum fighting ability of the test mice. In the fiber photometry recording, group-housed BALB/c male (>8 weeks) and female mice (>8 weeks) were used as stimulus animals.

Viruses

AAV2-EF1a-Flex-Chronos-GFP (3.6×10^{12} vg/ml), AAV2-Syn-Flex-ChrimsonR-tdTomato (6.0×10^{12} vg/ml), AAV2-hSyn-Flex-GFP (3.7×10^{12} vg/ml) were purchased from University of North Carolina vector core. AAV2-CAG-Flex-GCaMP6f-WPRE-SV40 (2.21×10^{13} vg/ml) was purchased from the University of Pennsylvania vector core facility. AAV5-Syn-Chronos-GFP ($\geq 5\times10^{12}$ vg/mL), AAV2-hSyn-DIO-hM4Di-mCherry (1.5×10^{13} vg/ml), AAV2-hSyn-DIO-mCherry (4×10^{12} vg/ml), and AAV9-Syn-ChrimsonR-tdTomato ($\geq 1\times10^{13}$ vg/mL) were purchased from Addgene. All viruses were aliquoted and stored at -80 °C until use.

METHOD DETAILS

Stereotaxic surgery

Mice were anesthetized with 1.5% isoflurane and placed in a stereotaxic apparatus (Kopf Instruments). Viruses were injected into the targeted brain regions using glass capillaries and a nanoinjector (World Precision Instruments, Nanoliter) at 10 nL/min.

For fiber photometry recording of $VMHvl^{Esr1}$ cells, 75 nL of AAV2-CAG-Flex-GCaMP6f-WPRE-SV40 was injected into the VMHvl (AP: -1.58 mm, ML: 0.775 mm, DV: 5.65 mm) of Esr1-Cre male mice. A 400-μm optical-fiber assembly (Thorlabs, FR400URT, CF440) was implanted 250 μm above the injection site and secured using dental cement (C&B Metabond, S380). During surgery, a head-fixation ring was also secured on the skull. All recordings started 3~5 weeks after the virus injection.

For slice recording experiments with Esr1-zsGreen male mice. 100 nl of AAV9-Syn-ChrimsonR-tdTomato was bilaterally injected into the PA (AP, -5.6mm; ML, 2.4mm; DV, -5.1mm). All mice were used for slice recording approximately four weeks after surgery, regardless of the length of RI tests. For slice recording of Esr1-Cre male mice in LTP and LTD induction experiments, 100 nL of 100 nl of AAV2-EF1a-Flex-Chronos-GFP was bilaterally injected into the PA (AP, -5.6mm; ML, 2.4mm; DV, -5.1mm), and 100 nL of AAV2-Syn-Flex-ChrimsonR-tdTomato was bilaterally injected into the VMHvl (AP, -4.85mm; ML, 0.776mm; DV, -5.75mm). The 200 μm

optic fibers (RWD Life Science, R-FOC-L200C-39NA) were bilaterally implanted 250 μm above the injection sites after virus injection and further secured with dental cement (C&B Metabond, S380). For the control group, 100 nL of AAV2-hSyn-Flex-GFP was bilaterally injected into the PA, and 100 nL of AAV2-hSyn-DIO-mCherry was bilaterally injected into the VMHvl. The light stimulation with LTP/LTD protocols and slice recording experiments were conducted four weeks after surgery. For slice recordings of qEPSC experiments, 100 nL of AAV2-Syn-Flex-ChrimsonR-tdTomato was bilaterally injected into the PA (AP, -5.6mm; ML, 2.4mm; DV, -5.1mm), and 100 nL of AAV2-EF1a-Flex-Chronos-GFP was bilaterally injected into the VMHvl (AP, -4.85mm; ML, 0.776mm; DV, -5.75mm) in Esr1-Cre male mice. For slice recording of sEPSC with hM4Di manipulation experiments, 100 nL of AAV2-hSyn-DIO-hM4Di-mCherry was injected into the VMHvl (AP, -4.85mm; ML, 0.776mm; DV, -5.75mm) bilaterally in Esr1-Cre male mice. The brains were used for recording at least three weeks after surgery. For initial checking of the LTP/LTD protocol using slice recording, 100 nL AAV5-Syn-Chronos-GFP was injected into the PA in C57 wild-type male mice.

For oLFP in vivo recording experiments, we injected 100 nL of AAV2-EF1a-Flex-Chronos-GFP into the PA and implanted an optrode into the VMHvl (AP, -4.7 to -4.85mm; ML, 0.776mm; DV, -5.5mm). The recording started approximately four weeks after surgery.

For testing changes in aggression after 10-day LTP protocol, we bilaterally injected 100 nL of AAV2-EF1a-Flex-Chronos-GFP into the PA (AP, -5.6mm; ML, 2.4mm; DV, -5.1mm), and 100 nL of AAV2-Syn-Flex-ChrimsonR-tdTomato into the VMHvl (AP, -4.85mm; ML, 0.776mm; DV, -5.75mm). The 200 μm optic fibers (RWD Life Science, R-FOC-L200C-39NA) were bilaterally implanted 250 μm above the injection sites after virus injection and further secured with dental cement (C&B Metabond, S380). For the control group, 100 nL of AAV2-hSyn-Flex-GFP was bilaterally injected into the PA, and 100 nL of AAV2-hSyn-DIO-mCherry was bilaterally injected into the VMHvl. The light stimulation with LTP protocols and behavior experiments were performed four weeks after surgery.

For drug infusion experiments, we implanted the bilateral cannula sets (RWD Life Science, center-to-center distance: 1.5mm) into the VMHvl (AP, -4.85mm; ML, 0.75mm; DV, -5.0mm). The behavior tests and slice recordings started at least one week after surgery.

Behavior tests and analysis

Resident-intruder tests

The test mice were always single-housed resident mice. In the daily winning training and aggression tests, a group-housed non-aggressive adult male BALB/c mouse randomly picked from a pool of 30 mice (housed 4-5 mice/cage) was introduced into the test mouse's home cage and allowed to interact freely with the resident mouse for 10 min. Resident mice that attacked the intruders within 10 minutes were identified as "Winners." Mice that did not attack during the 10-minute interaction were identified as "Social animals." Animals that attacked the intruder for 1 day, 5 consecutive days, and 10 consecutive days constitute 1d W, 5d W, and 10d W groups, respectively. In the 10d S group, mice showed no aggressive behaviors over the 10 days of RI tests. Animals that showed unstable aggression across days were excluded. In the RI probe test, an adult male DBA mouse (group-housed) was introduced into the home cage of the test mouse and immediately removed after the resident mouse attacked the DBA mouse. In the competition test, an adult male SW mouse (single-housed) was introduced into the test mouse's home cage and removed once the outcome was clear. The loser typically freezes in the corner, shows submissive postures, or escapes from the winner when approached. In contrast, the winner walks freely around the cage and initiates all attacks. For the loser groups, the test animals were introduced into the home cage of a single-housed, aggressive adult male SW mouse. Animals defeated by the SW resident for 1 day, 5 consecutive days, and 10 consecutive days, constituted 1d L, 5d L, and 10d L groups, respectively.

Locomotion test

We measured the animal's locomotion in its home cage and a large open field arena. In the home cage, the top-view videos were acquired using a camera (Balser, acA640-100gm) after removing the cage lid, water bottle, and food. Trajectories and distances traveled were analyzed by ANY maze software (ANY-maze). Locomotion tests in the open field were performed following the previously described method.[65] Each animal was placed into the center of the open field arena (40 cm x 40 cm x 35 cm) (Stoelting, #60101) illuminated at approximately 90 lux. The distance traveled over the 5 minutes was analyzed using ANY maze software.

Light-dark box test

The light-dark test was performed using a previously reported method with minor modifications.[66] The light-dark box consists of a starting dark box (W × L × H: 40 cm × 20 cm × 35 cm) and a lightbox (W × L × H: 40 cm × 20 cm × 35 cm), separated by a divider with an opening (Stoelting, #63101). Mice were placed into the start box with the opening blocked by a plastic plate. During the test, the plate was removed to allow the mouse to move freely between the boxes for 10 minutes. The time spent and the distance traveled in the light box were recorded and analyzed using the ANY Maze software.

Novelty-suppressed feeding test

Novelty-suppressed feeding tests were performed in the open field using a previously reported method with minor modifications.[67] Mice were food-deprived for 6 hours prior to the test. Food pellets were ground and sweetened with 50% sucrose water and then placed in a small round cap in the center of the arena. A petri dish (10 cm diameter) was placed under the cap to secure the cap. Each animal was placed into a corner of the open field arena (40 cm x 40 cm x 35 cm) (Stoelting, #60101) illuminated at approximately 90 lux. The latency to eat was calculated as the period from the test mouse introduction to the first time the animal entered the food zone and stayed there for over 2s. The food was weighed before and immediately after the test to calculate the amount of consumed food.

Animal tracking and behavior analysis

Animal behaviors were videotaped using a top-view camera (Edmund, 89533) controlled by StreamPix (Norpix) at 25 fps. For the animal tracking and locomotion analysis in the light-dark box test, home cage, and open field test, the recorded videos were analyzed offline using ANY-maze software. For RI, aggression probing, and competition tests, ''investigate'' and ''attack'' were manually annotated frame by frame using custom software written in MATLAB (https://pdollar.github.io/toolbox/). ''Investigate'' is defined as nose contact with any body part of the target mouse. ''Attack'' is defined as a series of actions by which the male mouse lunges, bites, chases, and pushes the target mouse.

Measure MUP and testosterone

Urine was collected and processed to determine MUP concentration as described previously.[68,69] The urine samples were stored at -20 °C after collection until analysis. We measured total protein and creatinine levels using QuantiChrom Protein Creatinine Ratio Assay Kit (BioAssay Systems, #DPCR-100) and calculated their ratio.

We followed a previous method to measure testosterone in the mouse tail blood.[70] Mice were anesthetized with 1.5% isoflurane and placed in a stereotaxic apparatus. We then collected the tail blood and centrifugated it (4 °C, 1500 RCF) for 10 minutes to isolate the serum. The serum was stored at -80 °C until all samples were collected. We then measured the testosterone levels in the serum using an ELISA Kit (Crystal Chem, #80552) based on the manufacturer's instructions.

Fiber photometry recording

The fiber photometry setup was as we previously described.[9,51] Briefly, a 390-Hz sinusoidal blue LED light (30 μW) (LED light: M470F1; LED driver: LEDD1B; both from Thorlabs) was bandpass filtered (passing band: 472 ± 15 nm; FF02-472/30-25, Semrock) and delivered to the brain to excite GCaMP6f. The emission lights traveled back through the same optical fiber, were bandpass filtered (passing bands: 535 ± 25 nm; FF01-535/505, Semrock), passed through an adjustable zooming lens (SM1NR01, Thorlabs; Edmun optics no. 62-561), were detected by a Femtowatt Silicon Photoreceiver (Newport, 2151) and recorded using a real-time processor (RZ5, TDT). The envelope of the 390-Hz signals reflected the intensity of GCaMP6f and was extracted in real-time using a custom TDT OpenEX program. The signal was low-pass filtered with a cut-off frequency of 5 Hz.

Three to four weeks after surgery, the mice were habituated to head fixation for at least 3 days, 30 minutes a day. On the day of recording, the mice were head-fixed, and an anesthetized male or female Balb/C mouse or a toy mouse was delivered to ~2 mm in front of the nostrils of the recording mouse using a linear track 6 times, each for 10 s and spaced by 60 s (2 minutes in between male and female mice or between the female mouse and toy mouse). The responses of the $VMHvl^{Esr1}$ cells to sensory cues were recorded for 3 days to ensure that the signal was stable. Then, the mice underwent repeated winning or social interaction in a daily 10-minute RI test. The neural responses to various stimuli to headfixed animals were probed on the day after 1, 5, and 10 days of RI tests. The head-fixed photometry recording was carried out 4-6 hours before the RI test if they were conducted on the same day. All the recordings were done at a similar time of the day throughout the experiment.

To analyze the recording data, the MATLAB function 'msbackadj' with a moving window of 25% of the total recording duration was first applied to obtain the instantaneous baseline signal. The instantaneous ΔF/F value was calculated as $(F_{raw}-F_{baseline})/F_{baseline}$. The post-stimulus histograms (PSTHs) of ΔF/F aligned to the onset of each stimulus presentation were constructed for each mouse and then averaged across mice. The average ΔF/F response was calculated as the mean ΔF/F signal during the stimulus delivery period, averaged first across trials and then animals.

oLFP recording

We followed our previously published method for optrode recording in freely moving mice.[8,71] Briefly, a movable bundle containing 16 tungsten microwires (13 μm in diameter each; California Fine Wire) and a 100-μm optical fiber (RWD Life Science, R-FOC-BL100C-22NA) was implanted into the VMHvl during surgery. We also used a simplified unmovable optrode that was constructed by attaching a single tungsten electrode (MicroProbes for Life Science, WE30030.5A3) to a 100-um optic fiber. The recorded signal was amplified using a head-mounted headstage (Tucker Davis Technology, LP16CH), passed through a torqueless, feedback-controlled commutator (Tucker Davis Technology, AC32), and digitized using a commercial amplifier (RZ5, Tucker Davis Technology).

Four weeks after surgery, we connected the implanted electrode with the headstage and delivered 0.5 - 2 mW, 5 ms, 0.1 Hz, 470 nm light pulses (Shanghai Dream Lasers Technology) to probe the oLFP. The animal then underwent a 10-minute RI test. Afterward, the oLFP was again probed. The procedure was repeated for 10 days. The light intensity for probing the LFP stayed constant across days for each animal.

To determine the oLFP change after the LTP and LTD stimulation protocol, we first probed the oLFP responses using 0.5 - 2 mW, 5 ms, 0.1 Hz, 470 nm light pulses for 3-5 min. We then applied the LTP protocol (530 nm, ~1.3 mW, 20 Hz, 5 ms, 25 s on and 5 s off for 3 times) or LTD protocol (530 nm, ~0.13 mW, 1 Hz, 5 ms, 600 s) (Changchun new industries optoelectronics technology). Immediately after the LTP or LTD stimulation protocol was completed, we again probed the oLFP for 5-10 min. To understand whether the LTP protocol-induced oLFP change accumulates over days, we performed LTP stimulation once a day for 10 consecutive days and probed the oLFP response daily before applying the LTP protocol.

In vivo optogenetic modification of PA-VMHvl pathway

The implanted optical fibers (RWD Life Science, R-FOC-L200C-39NA) were connected with 200 μm multimode patch cords (Thorlabs, FT200EMT) through matching sleeves (Thorlabs, ADAL1) to deliver light. Four weeks after the surgery, we habituated the animals to the head fixation and optic fiber connecting procedures several times. For behavioral experiments, the light was delivered bilaterally daily for 10 days. For slice recording, we unilaterally applied the LTP stimulation protocol (530 nm, ∼2 mW, 20 Hz, 5 ms, 25 s on, 5 s off, 3 times) for 1, 5, and 10 days. All animals were single-housed and did not encounter any intruder. To assess the effect of blocking PA-VMHvl potentiation on winning-induced plasticity, we subjected the test animal to an RI test with a BC intruder for 10 minutes. Then, for animals that won the RI tests, we applied the LTD stimulation protocol (1Hz, ∼0.5 mW, 5ms, 600s) unilaterally immediately after the RI test for 1 day or 10 consecutive days.

NMDA receptor antagonist injection

To block NMDA receptor in the VMHvl, we implanted a bilateral guide cannula (RWD Life Science, #62057) 0.7 mm above the pVMHvl. For the unilateral NMDAR blockade experiment, animals underwent the 10-min RI test on day 1. Immediately after the RI test, we injected 250 nL of D-APV (1μg, Tocris, #0106) into one side of the implanted cannula using a 10 μl syringe (Hamilton, #58380-U) attached to a plastic tube and an injector (RWD Life Science, #BC-22, #62521, and #62228). 250 nL of the vehicle was injected into the other side of the VMHvl. Animals were sacrificed the next day, and VMHvl cells were recorded from both APV- and Veh-injected sides. For the bilateral NMDAR blockade experiment, we injected 250 nL/side of D-APV or vehicle into the VMHvl bilaterally after the first day RI test and tested the behavior of the animals in the RI tests for 3 consecutive days.

Patch-clamp slice electrophysiological recording

All the slice recordings were performed on the day after the final behavior test or light stimulation and, if applicable, three to four weeks after the virus injection. Mice were anesthetized with isoflurane, and the brains were submerged in the oxygenated ice-cold cutting solution containing (in mM) 110 choline chloride, 25 $NaHCO_3$, 2.5 KCl, 7 $MgCl_2$, 0.5 $CaCl_2$, 1.25 NaH_2PO_4, 25 glucose, 11.6 ascorbic acid and 3.1 pyruvic acid. The coronal VMHvl brain sections (275 μM in thickness) were cut using the Leica VT1200s vibratome and collected into the oxygenated artificial cerebrospinal fluid (ACSF) solution containing (in mM) 125 NaCl, 2.5 KCl, 1.25 NaH_2PO_4, 25 $NaHCO_3$, 1 $MgCl_2$, 2 $CaCl_2$ and 11 glucose at 32-34 °C and incubated for 30 min. Then, the sections were transferred to room temperature until use. During recording, we moved a VMHvl section into the recording chamber perfused with oxygenated ACSF and performed the whole-cell recordings. The recorded signals were acquired with MultiClamp 700B amplifier (Molecular Devices) and digitized at 20 kHz using DigiData1550B (Molecular Devices). The stimulation and recording were conducted using the Clampex 11.0 software (Axon instruments). The intracellular solution for current-clamp recording contained (in mM) 145 K-gluconate, 2 $MgCl_2$, 2 Na_2ATP, 10 HEPES, 0.2 EGTA (286 mOsm, pH 7.2). The intracellular solution for the voltage clamp recording contained (in mM) 135 $CsMeSO_3$, 10 HEPES, 1 EGTA, 3.3 QX-314 (chloride salt), 4 Mg-ATP, 0.3 Na-GTP, and 8 sodium phosphocreatine (pH 7.3 adjusted with CsOH). The recorded data were analyzed using Clampfit (Molecular Devices).

Esr1 cells in the VMHvl were labeled with zsGreen and identified with an Olympus 40× water-immersion objective with a GFP filter. The cell membrane potential was held at -70 mV to record the sEPSCs, mEPSCs, and oEPSCs, and 0 mV to record sIPSCs, mIPSCs, and oIPSCs. For mEPSCs and mIPSCs recordings, we bath applied 1μM tetrodotoxin citrate (TTX, Tocris). To activate the Chronos- or ChrimsonR-expressing axons in the VMHvl, 0.1Hz, 1ms, 470nm, or 605nm light pulses (pE-300 white; CoolLED) were delivered to the recorded sections through the objective. To determine the AMPA and NMDA receptor-mediated currents, we bath applied 2 μM SR-95531 (a $GABA_A$ receptor antagonist) and held the cells at -70 mV for AMPAR-mediated current recording and +40 mV for NMDAR-mediated current recording. The AMPAR-mediated current was the maximum value of the EPSC trace. The NMDAR-mediated current was calculated as the average value between 60 and 65 ms after the light onset. In the LTP and LTD induction experiments (Figures S5R–S5Z), the cells were recorded blindly within the VMHvl (without zsGreen guidance). We probed the oEPSCs using 0.1Hz, 1ms, 470nm LED light delivered through the objective for 3min (∼20 trials), and then delivered a train of light pulses (20Hz, 5ms, 25s, 5s interval, 3 times), and then probed oEPSCs for 10min after stimulation. In the LTD experiments, we delivered 1Hz, 5ms, 470nm light for 600s after 3 min probing of oEPSCs. We also recorded the oEPSCs for 10 min after light stimulation.

We performed current-clamp recordings to determine the intrinsic excitability of $VMHvl^{Esr1}$ cells. We recorded the voltage changes of the cells in response to a series of 500ms current steps from -20 pA to 150 pA in 10 pA increments. In addition, the intrinsic properties of each cell, such as rheobase, resting potential, input resistance, and AP threshold, were characterized. The rheobase was defined as the minimum current capable of inducing the first action potential. The resting potential was measured directly after rupturing the cell membrane with 0 pA holding current. The input resistance was read from the membrane test window of the software after membrane break-in during recording (Clampex 11.0 software). The AP threshold for the spike of each neuron was calculated as the voltage at which $\Delta V/\Delta t$ reached 5% of the maximum AP rise slope.

For the sEPSC recordings in hM4Di-expressing mice, the cell was held at -70mV, and sEPSCs were recorded before and after 10 min 10 μM CNO perfusion. For the light-evoked qEPSC recordings, Ca^{2+} in ACSF was replaced with 4mM Sr^{2+}, 1 μM TTX and 100 μM 4AP were added to the ACSF before recording. 605 nm and 470 nm light pulses (1ms, 0.1Hz) were delivered to elicit the glutamate release from PA^{Esr1} and $VMHvl^{Esr1}$ cells, respectivley. We detected the evoked qEPSCs 0.5-1.5s after the light onset and calculated the average number of qEPSCs from 5 sweeps using Clampfit 11 (Molecular Devices).

Dendritic spine labeling and imaging

To obtain the cell dendritic spine morphology, we added 1% biocytin (Tocris) to the internal solution of whole-cell patch-clamp recording and recorded the cell for at least 15 min before withdrawing the electrode. After the recording, the sections were fixed using 4% paraformaldehyde overnight. The free-floating brain sections were washed 3 times with phosphate-buffered saline (PBS) (10 min), followed by 1 hr blocking in 0.3% NDS PBST (0.3% Triton X-100 in PBS with 10% normal donkey serum) at room temperature. The sections were then incubated with Alexa Fluor 647 conjugated streptavidin (Thermo Fisher Scientific, 1:250 dilution) in 0.3% NDS PBST at 4°C for 72 h. The sections were washed with 1× PBS and mounted onto super-frost slides (Thermo Fisher Scientific, 12-550-15). The z-stack images of dendritic spine segments were acquired using a confocal microscope (Zeiss LSM 700 microscope) with 64× oil objective with 0.18 μm step size. The different types of spines were identified and classified using Neurolucida 360 (MBF Bioscience). Five dendritic segments were analyzed for each cell, and the averaged data were used for further comparisons across groups.

Immunohistochemistry

Esr1-zsgreen mice were perfused transcardially with PBS, followed by 4% paraformaldehyde in PBS. The brains were extracted, post-fixed in 4% PFA for 2 ~3 hours at 4 °C followed by 48 hours in 30% sucrose, and then embedded in OCT compound (Fisher Healthcare) and frozen on dry ice. 50 μm thick coronal brain sections were cut using a cryostat (model #CM3050S, Leica Biosystems) and collected in PBS. After that, the brain slices were washed with PBS (1 × 10 minutes) and blocked in PBS-T (0.3% Triton X-100 in PBS) with 5% normal donkey serum (NDS, Jackson Immuno Research) for 30 minutes at room temperature. The slices were then incubated in primary antibody diluted in blocking solution (rabbit anti-Esr1, 1:10000, Millipore, Cat# 06-935) at 4 °C for 16- 20 hours, washed with PBS-T (3 × 10 minutes), incubated in secondary antibody and Nissl diluted in 5% NDS containing PBS-T (Cy3 donkey anti-rabbit IgG, 1:500, Jackson Immuno Research, Cat# 711-165-152; 435/455 Blue Fluorescent Nissl Stain, 1:200, Thermo Fisher Scientific, Cat# N21479) for 4 hours, and then washed with PBS-T (2 × 10 minutes). After drying, Slides were covered using a mounting medium (Fluoromount, Diagnostic BioSystems, #K024). Sections were imaged using a slide scanner (Olympus, VS120) and a confocal microscope (Zeiss, LSM 800).

QUANTIFICATION AND STATISTICAL ANALYSIS

No statistical methods were used to pre-determine sample sizes, but our sample sizes are similar to those reported in previous publications.[12,15,72,73] All experiments were conducted using 2-3 cohorts of animals. The results were reproducible across cohorts and combined for final analysis. Statistical analyses were performed using Prism10 (GraphPad Software). All statistical analyses were two-tailed. Parametric tests, including one sample t-test, paired t-test, unpaired t-test, and One-way ANOVA, were used if distributions passed Kolmogorov–Smirnov (for sample size $\geq$ 5) or Shapiro-Wilk tests (for sample size < 5) for normality or else nonparametric tests were used, including one sample Wilcoxon test, Wilcoxon matched-pairs signed rank test, Mann-Whitney test, and Kruskal-Wallis test. For comparisons across multiple groups and variables, Two-way ANOVA was used without formally testing the normality of data distribution. Following two-way ANOVA, differences between groups were assessed using Sidak's multiple comparison test or Tukey's multiple comparisons test based on the Prism recommendation. Two-sample Kolmogorov-Smirnov test was used to compare the distribution of two groups. When more than two one-sample t-tests were performed, the p values were adjusted using Holm-Šídák correction or FDR correction. All p values < 0.05 are indicated. If not specified, p>0.05. Error bars represent ± SEM. For detailed statistical results, including exact p values, F values, t values, degree of freedom, and cohort number, see Table S2.

Supplemental figures

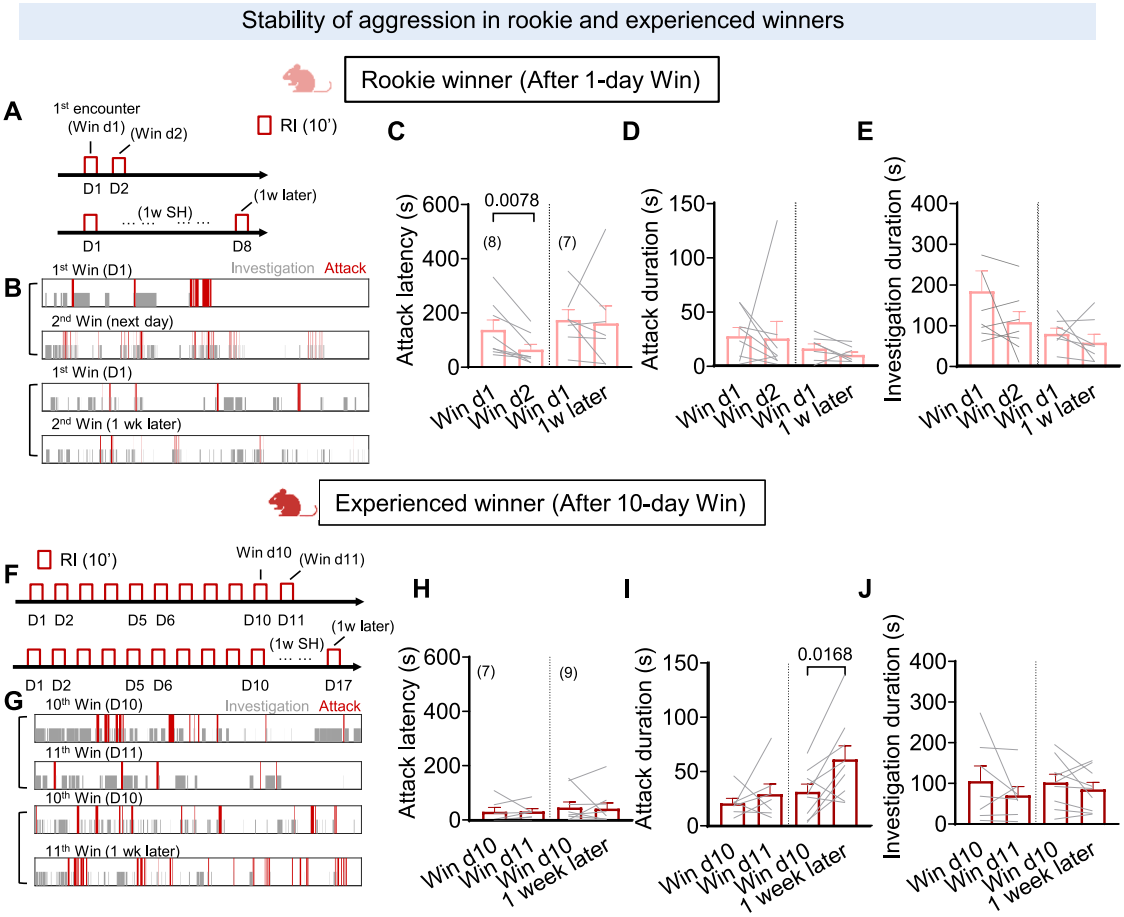

Figure S1. Stability of aggression in rookie and experienced winners, related to Figure 1

(A) Behavior paradigm to test aggression levels 1 and 8 days after 1 day of winning.

(B) Raster plots of attack and investigation during the RI tests 1 and 8 days after 1 day of winning.

(C–E) Latency to attack (C), attack duration (C), and investigation duration (E) during the first RI tests and second RI tests 1 and 8 days later.

(F) Behavior paradigm to test aggression levels 1 and 8 days after 10 days of winning.

(G) Raster plots of attack and investigation during the RI tests 1 and 8 days after 10 days of winning.

(H–J) Latency to attack (H), attack duration (I), and investigation duration (J) during the 10th RI tests and the 11th RI tests 1 and 8 days later.

Bars and error bars represent mean ± SEM. Lines represent individual animals. Numbers in parentheses indicate the number of subject animals. (C [win day 1 vs. win day 2], D [win day 1 vs. win day 2], and H and I [win day 10 vs. win day 11]) Wilcoxon matched-pairs signed rank test. (C [win day 1 vs. 1 week later], D [win day 1 vs. 1 week later], E and I [win day 10 vs. 1 week later], and J) Paired t test. All statistical tests are two-tailed. All $p \leq 0.05$ are specified. If not indicated, $p > 0.05$. See Table S2 for detailed statistics.

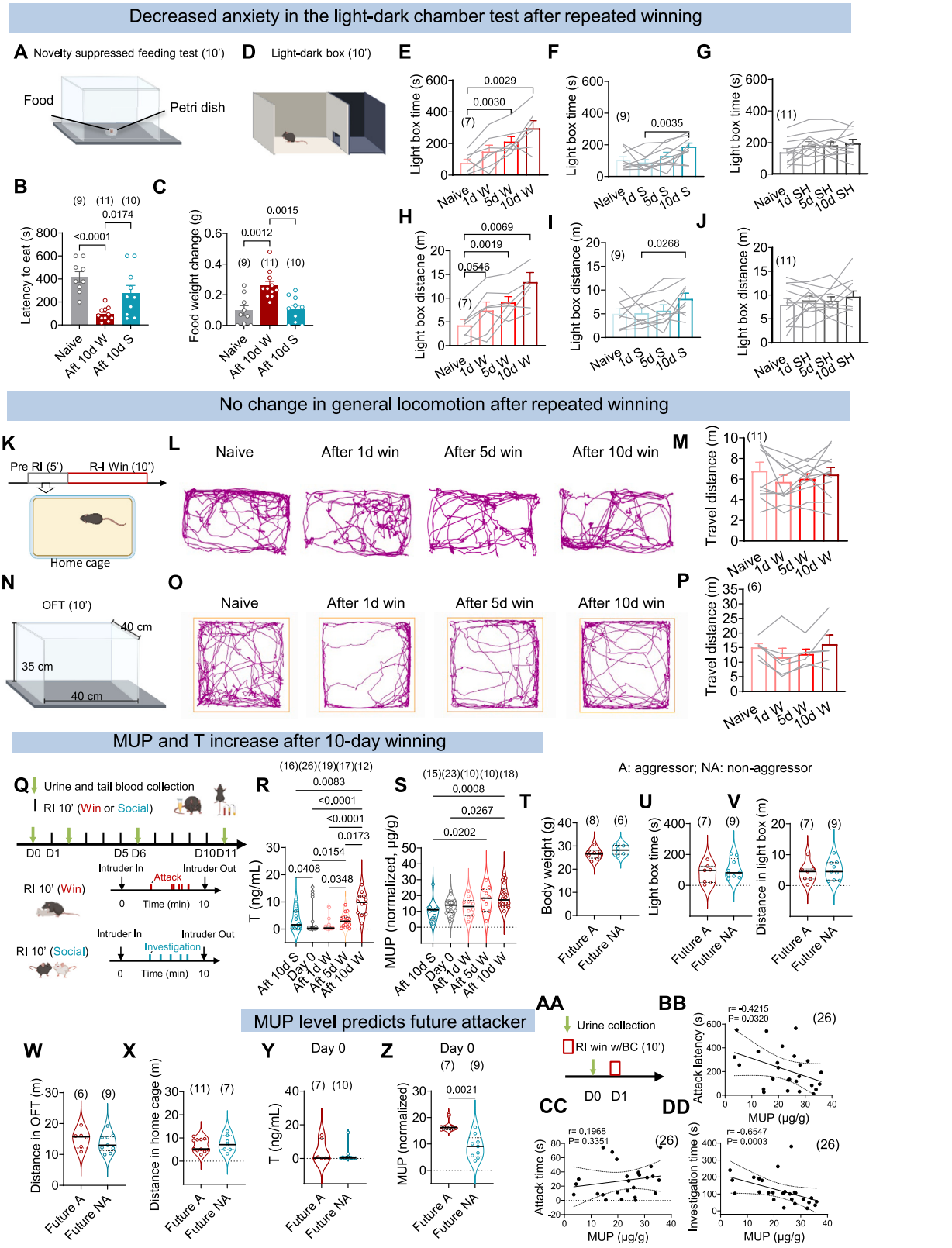

(legend on next page)

Figure S2. Changes in non-social behaviors, MUP, and T after repeated winning, related to Figure 1

(A) Schematic representation of the novelty-suppressed feeding test box.
(B and C) Latency to eat (B) and food weight change (C) in naive mice, 10-day social mice, and mice with 10 days of winning experiences.
(D) Schematic representation of the light-dark box.
(E–G) Time spent in the light box in mice with various days of winning experiences (E), social interactions (F), and single-housing (G).
(H–J) The total travel distance in the light box with various days of winning experiences (H), social interactions (I), and single-housing (J).
(K) Measuring the locomotion in the home cage (−5–0 min before the RI test).
(L) Representative tracking of the test animal's body center in the home cage after various days of winning.
(M) Travel distance in the home cage of mice with various days of winning experiences.
(N) Measuring the locomotion in an open field arena.
(O) Representative tracking of the test animal's body center in the open field arena after various days of winning.
(P) Travel distance in the open field of mice with various days of winning experiences.
(Q) Schematic representation of urine and blood collection in mice before and after 1, 5, and 10 days of winning and 10 days of social experiences against BC male intruders.
(R and S) Quantification of testosterone (R) and MUP (S) levels in mice before and after 1, 5, and 10 days of winning and 10 days of social experiences against BC male intruders.
(T–X) Body weight (T), time spent in the light box (U), travel distance in the light box (V), travel distance in the open field test (W), and travel distance in the home cage (X) in naive mice that attacked (future aggressors) and did not attack (future non-aggressors) during the RI test with BC male intruders on the next day.
(Y and Z) Testosterone level (Y) and MUP level (Z) of naive mice that attacked (future aggressors) and did not attack (future non-aggressors) during the RI test with BC male intruders on the next day after the sample collection.
(AA) Experimental timeline.
(BB–DD) Correlation between MUP and latency to attack (BB), attack duration (CC), and investigation duration (DD) on the first day of attack in test mice.
Black lines inside of the violin plots mark the median. Bars and error bars represent mean ± SEM. Circles and lines represent individual animals. Numbers in parentheses indicate the number of subject animals. (B and C) One-way ANOVA with Tukey's multiple comparisons test. (E–J, and P) One-way ANOVA with repeated measures followed by Tukey's multiple comparisons test. (M) Friedman test with repeated measures followed by Dunn's multiple comparisons test. (R and S) Kruskal-Wallis test followed by multiple comparison tests with false discovery rate (FDR) correction. (T–W) Two-tailed unpaired t test. (X–Z) Two-tailed Mann-Whitney test. (BB and CC) Pearson correlation coefficients test. (DD) Nonparametric Spearman correlation test. All r and p values are specified. All $p \leq 0.05$ are specified. If not indicated, $p > 0.05$.
See Table S2 for detailed statistics.

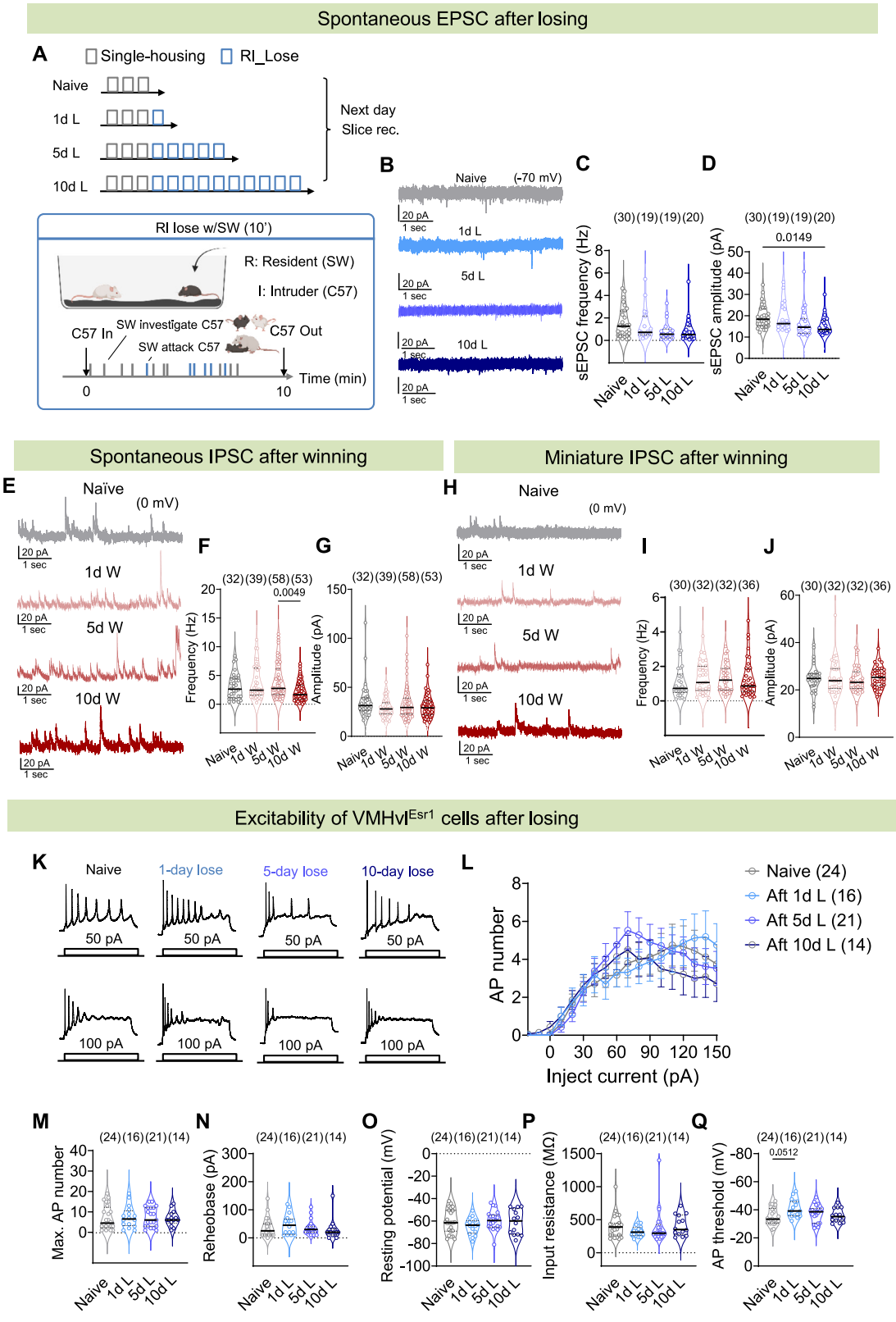

(legend on next page)

Figure S3. Additional characterization of physiological changes of VMHvl^{Esr1} cells after winning or losing experiences, related to Figures 3 and 6

(A) Experimental timeline and illustration of the RI tests during which C57 test mice were repeatedly defeated by SW male residents.
(B) Representative voltage-clamp recording traces of VMHvl^{Esr1} cells in mice after various losing experiences.
(C and D) Quantification of the frequency (C) and amplitude (D) of sEPSCs of VMHvl^{Esr1} cells in mice with 0, 1, 5, and 10 days of losing experiences.
(E) Representative voltage-clamp recording traces of VMHvl^{Esr1} cells in animals with various days of winning experiences. The holding potential is 0 mV.
(F and G) The sIPSC frequency (F) and amplitude (G) of VMHvl^{Esr1} cells in animals with various days of winning experiences.
(H) Representative voltage-clamp recording traces of VMHvl^{Esr1} cells in the presence of 1 μM TTX. The holding potential is 0 mV.
(I and J) The mIPSCs frequency (I) and amplitude (J) of VMHvl^{Esr1} cells in animals with various days of winning experiences.
(K) Representative current-clamp recording traces of VMHvl^{Esr1} cells with 50 and 100 pA current injections.
(L) F-I curve of VMHvl^{Esr1} cells in naive mice and mice with different days of losing experiences.
(M) Maximal numbers of action potentials across current steps of various groups.
(N–Q) Rheobase (N), resting membrane potential (O), input resistance (P), and AP threshold (Q) of VMHvl^{Esr1} cells in naive mice and mice with 1, 5, and 10 days of losing experiences.
Black lines inside of the violin plots mark the median. Circles represent individual cells. Numbers in parentheses indicate the number of recorded cells. (C, D, F, G, I, J, M, N, P, and Q) Kruskal-Wallis test with Dunn's multiple comparisons test. (L) Two-way ANOVA with Tukey's multiple comparisons test. (O) One-way ANOVA followed by Tukey's multiple comparisons test. All $p \leq 0.05$ are specified. If not indicated, $p > 0.05$.
See Table S2 for detailed statistics.

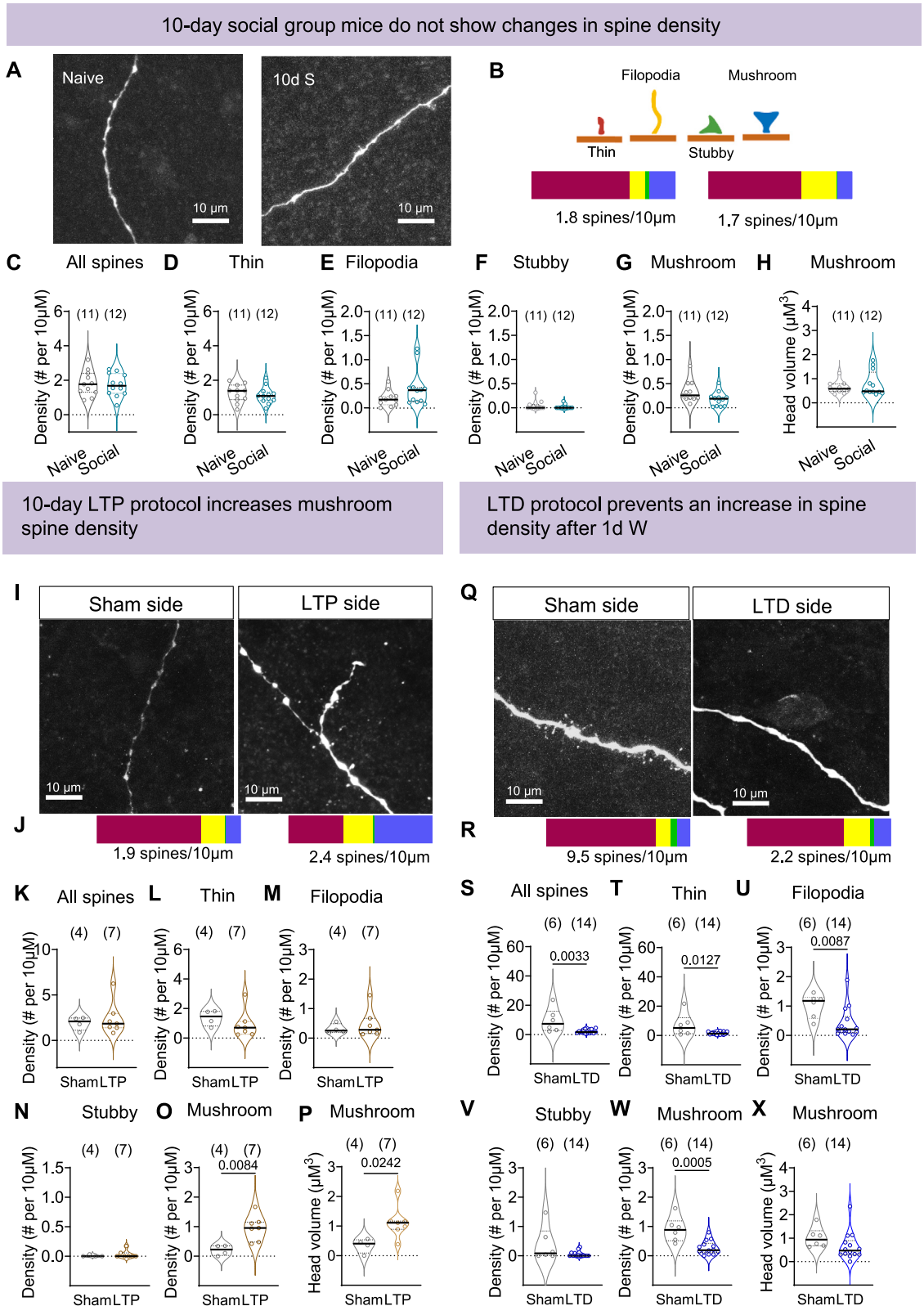

(legend on next page)

Figure S4. Spine morphology of VMHvl^{Esr1} cells after repeated social interaction, LTP, and LTD protocols, related to Figures 3 and 7

(A) Representative images of VMHvl^{Esr1} cell dendrites in naive (left) and 10-day social (right) animals.
(B) Schematic illustration of different types of spines (top) and their proportions in naive and 10-day social groups (bottom).
(C) Total spine density in naive and 10-day social groups.
(D–G) The density of thin spines (D), filopodia (E), stubby spines (F), and mushroom spines (G) in naive and 10-day social groups.
(H) The head volume of mushroom spines in naive and 10-day social groups.
(I) Representative images of VMHvl^{Esr1} cell dendrites on the sham and 10-day LTP stimulation sides.
(J) The proportion of different types of spines on sham and 10-day LTP sides.
(K) Total spine density of cells on the sham and 10-day LTP side.
(L–O) The density of thin spines (L), filopodia (M), stubby spines (N), and mushroom spines (O) of cells on the sham and 10-day LTP side.
(P) The head volume of mushroom spines of VMHvl^{Esr1} cells on the sham and 10-day LTP side.
(Q) Representative images of VMHvl^{Esr1} cell dendrites on the sham and LTD stimulation sides of a 1-day winning mouse.
(R) The proportion of different types of spines on sham and LTD sides.
(S) Total spine density of cells on the sham and LTD sides of 1-day winning mice.
(T–W) The density of thin spines (T), filopodia (U), stubby spines (V), and mushroom spines (W) of cells on the sham and LTD sides of 1-day winning mice.
(X) The head volume of mushroom spines of cells on the sham and LTD sides.
Black lines inside of the violin plots mark the median. Circles represent individual cells. Numbers in parentheses indicate the number of cells. (C, D, G, K–M, O, S, T, W, and X) Unpaired t test. (E, F, H, N, P, U, and V) Mann-Whitney test. All statistical tests are two-tailed. All $p \leq 0.05$ are specified. If not indicated, $p > 0.05$. See Table S2 for detailed statistics.

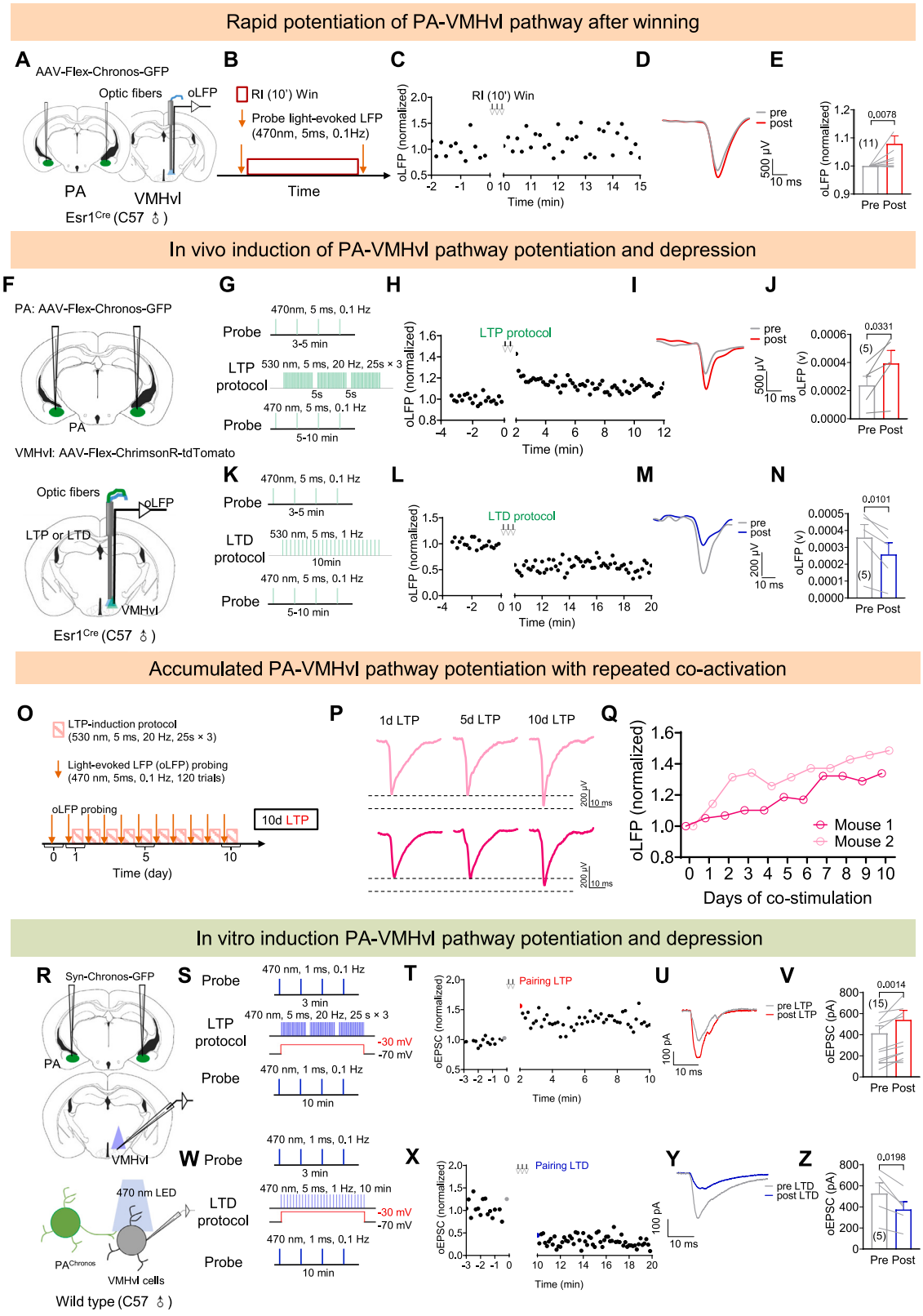

(legend on next page)

Figure S5. LTP and LTD stimulation effectively alter PA-VMHvl connection strength, related to Figure 7

(A) Experimental design for *in vivo* probing of VMHvl LFP evoked by PA terminal stimulation.
(B) Experimental timeline.
(C) Representative normalized oLFP before and after winning a BC male intruder in the 10-min RI test.
(D) Averaged oLFP traces of a representative animal before and after winning.
(E) Normalized amplitude of oLFPs before and after winning.
(F) Experimental strategies for *in vivo* manipulation of PA-VMHvl connection strength.
(G) *In vivo* light delivery protocol for LTP induction and oLFP probing.
(H) Normalized oLFP amplitude before and after LTP induction of a representative animal.
(I) Averaged traces of oLFP before and after LTP induction of a representative animal.
(J) oLFP amplitude before and after LTP induction of all animals.
(K) *In vivo* light delivery protocol for LTD induction and oLFP probing.
(L) Normalized oLFP amplitude before and after LTD induction of a representative animal.
(M) Averaged traces of oLFP before and after LTD induction of a representative animal.
(N) oLFP amplitude before and after LTD induction of all animals.
(O) Experimental timeline for 10-day *in vivo* LTP induction.
(P) Example trace of oLFP after 1, 5, and 10 days of LTP induction.
(Q) Normalized oLFP amplitude over 10 days of LTP induction. The probing occurred before the daily LTP induction.
(R) Experimental design for *in vitro* measuring of VMHvl cell EPSC evoked by PA terminal stimulation.
(S) *In vitro* light delivery and voltage step protocol for LTP induction and oEPSC recording.
(T) Normalized oEPSC amplitude before and after LTP induction of a representative cell.
(U) Representative oEPSCs (the gray and red dots in T) before and after LTP induction.
(V) oEPSC amplitude before and after LTP induction. The amplitude was calculated as an average of the last 5 EPSC traces before induction and the first 5 EPSC traces after induction.
(W) *In vitro* light delivery and voltage step protocol for LTD induction and oEPSC recording.
(X) Normalized oEPSC amplitude before and after LTD induction of a representative cell.
(Y) Representative oEPSCs (the gray and blue dots in X) before and after LTD induction.
(Z) oEPSC amplitude before and after LTD induction. The amplitude was calculated as an average of the last 5 EPSC traces before induction and the first 5 EPSC traces after induction.
Bars and error bars represent mean ± SEM. Lines in (E), (J), and (N) represent individual animals. Lines in (V) and (Z) represent individual cells. Numbers in parentheses in (E), (J), and (N) indicate the number of subject animals. Numbers in parentheses in (V) and (Z) indicate the number of recorded cells. (J, N, V, Z) Paired t test. (E) One sample Wilcoxon test. All statistical tests are two-tailed. All $p \leq 0.05$ are specified. If not indicated, $p > 0.05$.
See Table S2 for detailed statistics.

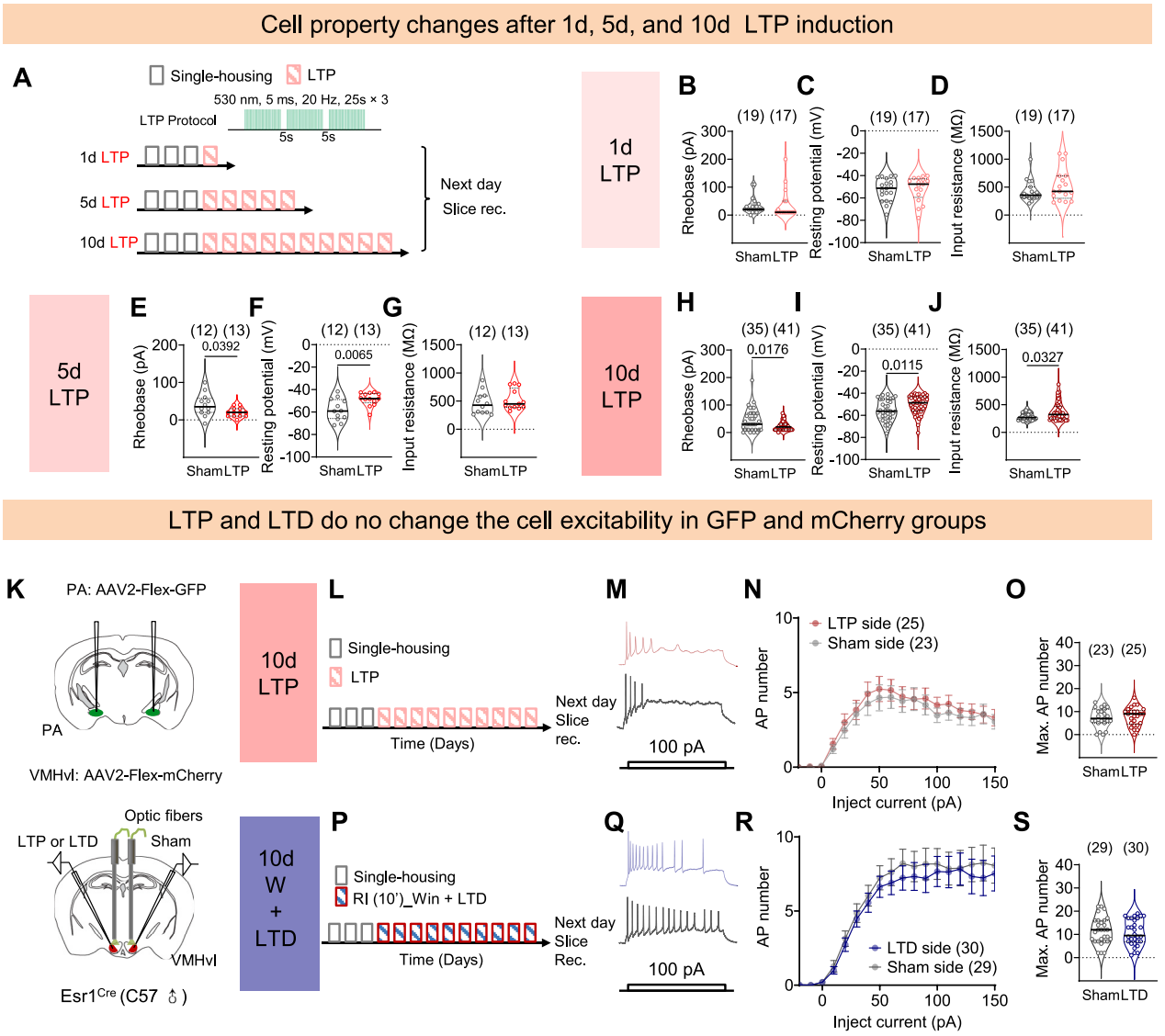

Figure S6. Intrinsic properties of VMHvl^{Esr1} cells after LTP induction and control group results, related to Figure 7

(A) Experimental timeline.

(B–D) The rheobase (B), resting potential (C), and input resistance (D) of VMHvl^{Esr1} cells on the sham and 1-day LTP induction sides.

(E–G) The rheobase (E), resting potential (F), and input resistance (G) of VMHvl^{Esr1} cells on the sham and 5-day LTP induction sides.

(H–J) The rheobase (H), resting potential (I), and input resistance (J) of VMHvl^{Esr1} cells on the sham and 10-day LTP induction sides.

(K) Virus injection, fiber implantation, and slice recording strategies.

(L) Experimental timeline.

(M) Representative current-clamp recording traces of VMHvl^{Esr1} cells on the sham and LTP light delivery sides with 100 pA current injection.

(N) The F-I curve of cells recorded from the sham and 10-day LTP induction sides.

(O) Maximal number of action potentials across current steps of cells recorded from the sham and LTP induction sides.

(P) Experimental timeline.

(Q) Representative current-clamp recording traces of VMHvl^{Esr1} cells on the sham and LTD induction sides with 100 pA current injection.

(R) The F-I curve of cells recorded from the sham side and 10-day LTD stimulation side.

(S) Maximal number of action potentials across current steps of cells recorded from the sham and LTD induction sides.

Black lines inside of the violin plots mark the median. Circles represent individual cells. Numbers in parentheses indicate the number of recorded cells. (C, E, F, I, O, and S) Unpaired t test. (B, D, G, H, and J) Mann-Whitney test. (N and R) Two-way ANOVA with repeated measures followed by Sidak's multiple comparisons test. All statistical tests are two-tailed. All $p \leq 0.05$ are specified. If not indicated, $p > 0.05$.

See Table S2 for detailed statistics.

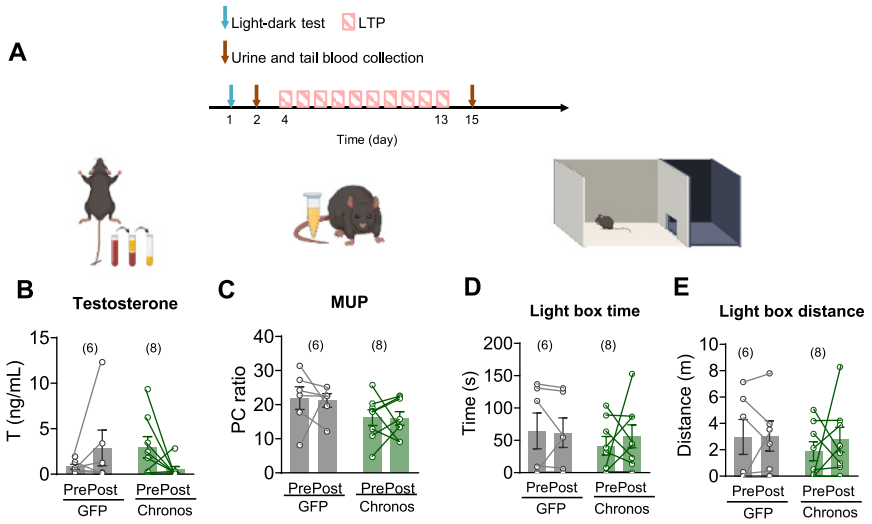

Figure S7. T and MUP levels and performance in the light-dark box do not change after 10 days of LTP induction, related to Figure 7

(A) Timeline for urine/blood collection and the light-dark test in mice subjected to 10-day LTP induction.

(B) The testosterone level before and after 10-day LTP stimulation in GFP- and Chronos-expressing mice.

(C) The normalized MUP level (urine protein to creatinine ratio) before and after 10-day LTP stimulation in GFP- and Chronos-expressing mice.

(D and E) The time spent (D) and distance traveled (E) in the light box before and after 10-day LTP stimulation.

Bars and error bars represent mean ± SEM. Circles and lines represent individual animals. Numbers in parentheses indicate the number of subject animals. (B–E) Two-way ANOVA with repeated measures followed by Sidak's multiple comparisons test. All $p \leq 0.05$ are specified. If not indicated, $p > 0.05$.

See Table S2 for detailed statistics.

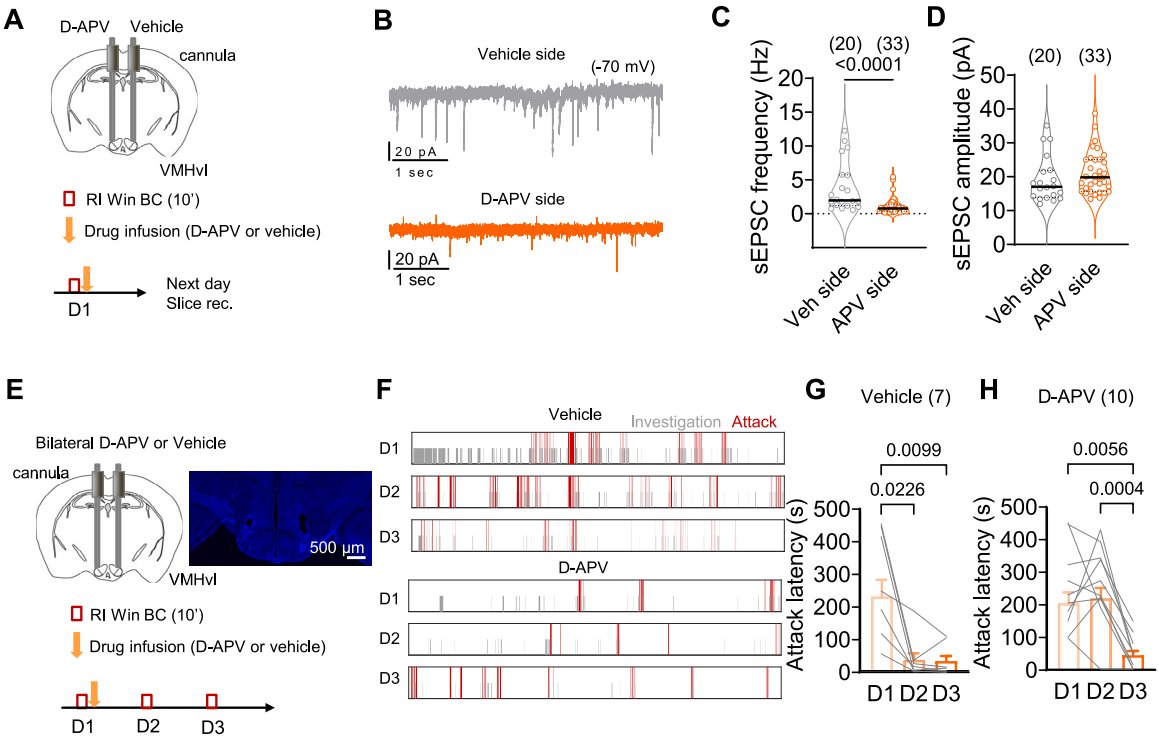

Figure S8. Antagonizing VMHvl NMDA receptor after winning blocks the VMHvl cell plasticity and the winner effect, related to Figure 7

(A) Schematic diagram of the cannula implantation and experimental timeline.

(B) Representative voltage-clamp recording traces on the vehicle- and APV-injected sides.

(C and D) Quantification of the frequency (C) and amplitude (D) of sEPSCs of VMHvl^{Esr1} cells on the vehicle- and D-APV-injected sides.

(E) Schematic diagram of the cannula implantation, a representative histology image, and experimental timeline.

(F) Raster plots showing attack and investigation during the RI test from day 1 to day 3 of representative animals in vehicle and D-APV groups.

(G and H) Latency to attack during the RI test from day 1 to day 3 of vehicle group (G) and D-APV group (H).

Black lines inside of the violin plots mark the median. Bar and error bar: mean ± SEM. Circles in (C) and (D) represent individual cells. Lines in (G) and (H) represent individual animals. Numbers in parentheses indicate the number of recorded cells or animals. (C and D) Two-tailed Mann-Whitney test. (G) Friedman test with repeated measures followed by Dunn's multiple comparisons test. (H) One-way ANOVA with repeated measures followed by Tukey's multiple comparisons test. All $p \leq 0.05$ are specified. If not indicated, $p > 0.05$.

See Table S2 for detailed statistics.